Universidade de Aveiro
Ano 2017

Departamento de Química

PANIZ SOLTANI

SÍNTESE DE NOVOS MATERIAIS DE CARBONO PARA APLICAÇÕES EM SUPERCONDENSADORES

SYNTHESIS OF NOVEL CARBON MATERIALS FOR SUPERCAPACITOR APPLICATIONS

Universidade de Aveiro
Ano 2017

Departamento de Química

PANIZ SOLTANI

SÍNTESE DE NOVOS MATERIAIS DE CARBONO PARA APLICAÇÕES EM SUPERCONDENSADORES

SYNTHESIS OF NOVEL CARBON MATERIALS FOR SUPERCAPACITOR APPLICATIONS

Dissertação apresentada à Universidade de Aveiro para cumprimento dos requisitos necessários à obtenção do grau de Mestre em Química/Functionalized Materials and Engineering (FAME), realizada sob a orientação científica do Prof. Doutor Rui Ramos Ferreira e Silva, Professor Associado do Departamento de Engenharia de Materiais e Cerâmica da Universidade de Aveiro e do Professor Catedrático Dr Klaus Mullen do Max Planck Institute of Technology for Polymer Research.

o júri

presidente

Prof.ª Doutora Ana Margarida Madeira Viegas de Barros Timmons
professora auxiliar do Departamento de Química da Universidade de Aveiro

Prof. Doutor Luís Manuel Cadillon Martins Costa
professor associado com agregação do Departamento de Física da da Universidade de Aveiro

Prof. Doutor Rui Ramos Ferreira e Silva
professor associado do Departamento de Engenharia de Materiais e Cerâmica da Universidade de Aveiro

agradecimentos

First I want to thank FAME program for providing a huge opportunity for us to be able to not just study but gain life experience.
I would also like to cordially thank Prof. Ana Barros, our coordinator in university of Aveiro, for being very supportive and helpful through all the process.
I would like to extend my thanks to Prof. Rui Silva for being supportive and helpful and letting me pursue my interests.
I am very grateful to Prof. Klaus Müllen for giving me a chance to work in his research group in Max Planck Institute in Mainz and let me learn from his great achievements.
I would also like to thank our project leader, Dr. Akimitsu Narita for always being available and going extreme ways to help me.
I am very thankful to Dr. Zhaoyang Liu for guiding me with this project and introducing me to the concept with his valuable knowledge.
I would like to next acknowledge all the cooperation partners in the Max Planck Institute of technology for Polymer Research in Mainz inside and outside our research group for great support.
I also want to thank:
Uwe Rietzler for teaching me AFM measurements.
Gunnar Glasser for SEM measurements.
Gabi Hermann for kindly providing the space and equipment in her lab.
Michael Steiert for XRD measurements.
Dr. Gang Wang for providing the mesoporous carbon spheres.
Dr. Seul Lee for providing RuO_2 nanosheets.
I am very thankful to my colleagues and office-mates for providing a friendly and environment for me and for all their help thorough this time specially Anna Baun, Bastian Dumslaff and Dr. Tim Dumslaff.
I also wanted to mention my very good friend Navid Khazaei for all his help and support through the good and bad times.
And last but for sure not least, I want to thank my family for raising me such that I had the possibility to have all these experiences, for always being there for me to rely on and for creating a “home” for me to miss and a “love” for me to go back to. Their happiness is my best reward.

palavras-chave

Micro-supercondensadores, armazenamento de energia, grafeno electroquimicamente exfoliado, *spin-coating*

resumo

Micro-supercondensadores (MSCs) são os principais componentes de dispositivos eletrónicos miniaturizados, portáteis e utilizáveis no vestuário. Embora muitos avanços tenham sido feitos neste campo nos últimos anos, a densidade de energia dos micro-supercondensadores permanece aquém das baterias de iões de lítio e dos condensadores eletrolíticos. Muitos esforços foram feitos para melhorar os desempenhos dos MSCs, como e fabricação de nanoestruturas e as tecnologias de filmes finos. Neste trabalho estudam-se MSCs baseados em carbono poroso e PEDOT:PSS, bem como de RuO_2 e grafeno electroquimicamente exfoliado. A combinação de materiais com capacitância de camada dupla pseudo-capacitiva e eletroquímica permite obter MSCs com uma capacitância até 1 $mF.cm^{-2}$ e capacidade até 51 $F.cm^{-3}$ nos dispositivos baseados em grafeno e capacitância até 203 $\mu F.cm^{-2}$ e capacitância de 12 $F.cm^{-3}$ nos dispositivos baseados em polímero. Ambos os dispositivos podem ser operados até 1000 $V.s^{-1}$, um valor cerca de três ordens de grandeza maior do que o das baterias convencionais. A elevada capacitância foi obtida com baixas taxas de varrimento (~ 10 $mV.s^{-1}$) com retenção de aproximadamente 40%.

keywords Micro-supercapacitors, energy storage, electrochemically exfoliated graphene, spin-coating

abstract Micro-supercapacitors (MSCs) are the key components of miniaturized, portable and wearable electronic devices. Although many advances have been made in this field during the recent years, micro-supercapacitors energy density remains far from those from lithium-ion batteries and electrolyte capacitors. Many efforts have been made to improve MSCs performances such as fabrication of nanostructures and thin-film manufacture technologies. Here, we demonstrated MSCs based on porous carbon and PEDOT: PSS polymer as well as RuO_2 and electrochemically exfoliated graphene. Combining materials with pseudo capacitive and electrochemical double layer capacitance ability, the resulting MSCs deliver an area capacitance up to 1mFcm^{-2} and stack capacitance up to 51 Fcm^{-3} for graphene based devices and area capacitance up to 203 µFcm^{-2} and stack capacitance up to 12 Fcm^{-3} for polymer based devices. Both devices show ability to be operated in ultra-high rates up to 1000 Vs^{-1} which is around three orders of magnitude higher that of conventional batteries. The high capacitance is generally obtained at low scan rates (~ 10 mVs^{-1}) and 40% of capacitance retention has been observed.

Table of Content

Index of Figures

Index of Tables

AFM	Atomic Force Microscopy
CV	Cyclic Voltammetry
DMF	N,N'- dimethylformamide
EC	Electrochemical Capacitors
EDLC	Electric Double-Layer Capacitor
EDL	Electric Double Layer
EDX	Energy Dispersive X-Ray Spectroscopy
EG	Exfoliated Graphene
EIS	Electrochemical Impedance Spectroscopy
GCD	Galvanostatic Charge/Discharge
MSC	Micro-supercapacitor
PANI	Polyaniline
PVA	Poly (vinyl alcohol)
SEM	Scanning Electron Microscopy
TBA	Tetrabutylammonium
XRD	X-Ray Diffraction

Chapter 1

Literature Review

1.1 Motivation and Objectives

This work was carried out to obtain micro-supercapacitors (MSCs) based on poly (3,4-ethylenedioxythiophene):poly (styrenesulfonate) (PEDOT:PSS) and mesoporous carbon spheres and also, in a second part, MSCs based on electrochemically exfoliated graphene and ruthenium oxide.

In today's electronics, lithium ion batteries are the main used energy storage source, however, they have a rather slow power uptake or delivery performance and therefore new faster systems are needed which are having higher-power energy storage. In-plane MSCs are newly microelectrochemical devices which could replace batteries because of their faster charge and discharge rate, longer life cycle and being able to provide higher power densities compared to batteries and conventional capacitors.

Supercapacitors are mostly divided in three categories based on their charge storage mechanism: electric double-layer capacitors, pseudocapacitors and hybrid systems. In principle, pseudocapacitors offer high capacitance but they have low-cycle performance and their rate capability is rather low while electrical double layer provide relatively low capacitance but they can achieve rapid charge storage. Hybrid systems which combine positive features of both electric double-layer capacitors and pseudocapacitors are more interesting choice since they can achieve high power densities and energy in one device.

Based on previous research of the host group, at Max Planck Institute of Technology for Polymer Research in Mainz, PEDOT:PSS was chosen due to its high electrical conductivity, fast and stable redox reactions, solubility in water and strong film forming ability; electrical double layer behavior was introduced by using mesoporous carbon spheres with high specific surface area.

Graphene is a very attractive material to be used in high-power MSCs considering its properties such as high surface to volume ration, high electrical conductivity. However, graphene itself lacks pseudocapacitive behavior and is only capable of electrical double layer capacitance. Ruthenium oxide (RuO_2) is widely used in supercapacitors because of being electrically conductive and having the ability to change between three oxidation states and as a result it was chosen here to add a pseudocapacitive behavior to the device.

1.2 Literature Review

1.2.1 Energy Storage

Energy storage devices are starting to play a large part in our life as time passes due to the decreasing availability of fossil fuels and the need for renewable resources. Electrical energy storage systems such as batteries and electrochemical capacitors are in the lead these days with Li ion batteries being the best in terms of performance and price and energy density which can reach up to 180 W.h/kg. With the pace of the new electronics and every day growing demand for miniaturization, powerful microscale energy storage systems are considered as key components. Despite all the progress achieved so far, performance improvement is still essential to meet the higher requirements of future systems.

Electrochemical capacitors (ECs) have had a relative limited attention until recently as most researches have been focused on developing high-performance Li-ion and other advanced secondary batteries. The problem with Li-ion batteries is their slow power delivery or uptake and as a consequence, faster and higher-power storage systems are needed and the best choice for this are ECs [1]. ECs which are also known as supercapacitors (SCs) or ultracapacitors because of their extraordinarily high capacitance density are like all capacitors, they physically store charge [1]. But, these devices can be fully charged or discharged only in a few seconds and as a result much higher power delivery can be achieved for shorter times. However, their energy density is lower than in batteries. The charge storing mechanism in conventional electrolyte and electrostatic capacitors is based on low-surface area plates, while ECs use an electrode with high surface area and a liquid electrolyte to set up an electric double layer by ions.

Traditionally, a supercapacitor is assembled as a sandwich-like stack configuration of a cell composed of collector/electrode/separator/electrode/collector and enclosed by sealing and packaging materials (Fig. 1-1) [2]. The two electrodes are separated mechanically by a membrane which is ion-permeable and serves as a separator between two electrodes to prevent short circuit. The electrolyte is composed of a conductive liquid mixture of an organic or aqueous solvent that can migrate out and into the electrodes during charge and discharge process. The input/output terminals of electricity to an outside circuit are the metallic collectors which electrically connect the electrodes [3, 4].

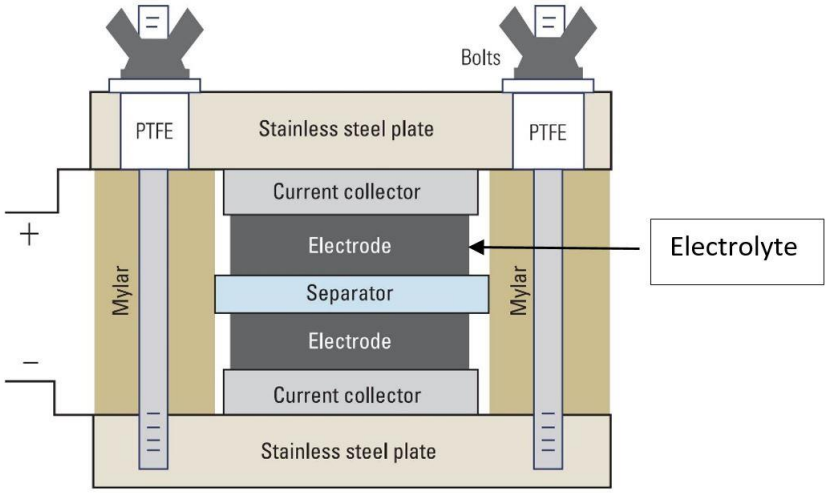

Fig.1-1. Scheme of the cell configuration in a supercapacitor [2]

Oppositely charged ions in the electrolyte settle on each electrode when a voltage is applied and they remain there when the voltage is turned off. There will be an electron current from negative electrode to balance the charges in the positive electrode when they are connected by a wire. Depending on the active material used as well as charge storage mechanism, several types of ECs can be distinguished [5].

There is a limit to the high capacitance for ECs, typically at a voltage around 1 to 3 V per cell, as the electrolyte undergoes chemical reactions and therefor the operating voltage cannot exceed that potential. Like batteries, ECs can also be series-connected for high voltage applications.To compare, batteries have the ability to store up to 30 times more charge for a given volume. However, with a similar size, ECs can deliver about thousands times more power. Moreover, unlike batteries, there is no change in volume because of the highly reversible electrostatic charge storage. One of the main causes of limited life cycle (around several hundred cycles) of batteries is because of this volume change in the active masses due to the redox reactions compared to millions of full charge-discharge cycles in ECs. In table 1-1 the main differences between batteries and ECs are compared [6].

Table 1-1. Comparison between batteries and ECs

Property	**Battery**	**Electrochemical Capacitor**
Storage mechanism	Chemical	Physical
Power limitation	Reaction kinetics, mass transport	Electrolyte conductivity
Energy Storage	High (bulk)	Limited (surface area)
Charge Rate	Kinetically limited	High, same as discharge rate
Cycle Life Limitations	Mechanical stability, Chemical reversibility	Side reactions

Recently, with the rapid progress of micro-scale devices such as implantable medical devices, micro-electrochemical devices and microrobots has encouraged the need for micro/-nano-scale power sources [7]. Currently, the most predominant used energy source for portable electronics these days, are micro-batteries [8]. However, with the mentioned drawbacks of batteries, micro-supercapacitors are considered as very good replacements having advantages like: fast charge/discharge rate, long cycle life and also being able to provide power densities several orders of magnitude higher than conventional supercapacitors and batteries [9].

Supercapacitors are mostly divided in three categories based on their charge storage mechanism (Fig.1-2) : (1) electric double-layer capacitors (EDLCs) that use high surface area carbon electrodes to electrostatically store charges on the interface (Fig. 1-3a); (2) pseudocapacitors that use reversible redox (faradaic) reactions to electrochemically store electrical energy, typically based on metal oxides or conductive polymers (Fig.1-3b); and (3) hybrid supercapacitors which are composed of asymmetric electrodes or special hybrid electrodes that have both pseudocapacitance of a transition metal oxide or conductive polymer and double-layer capacitance of carbon [10, 11].

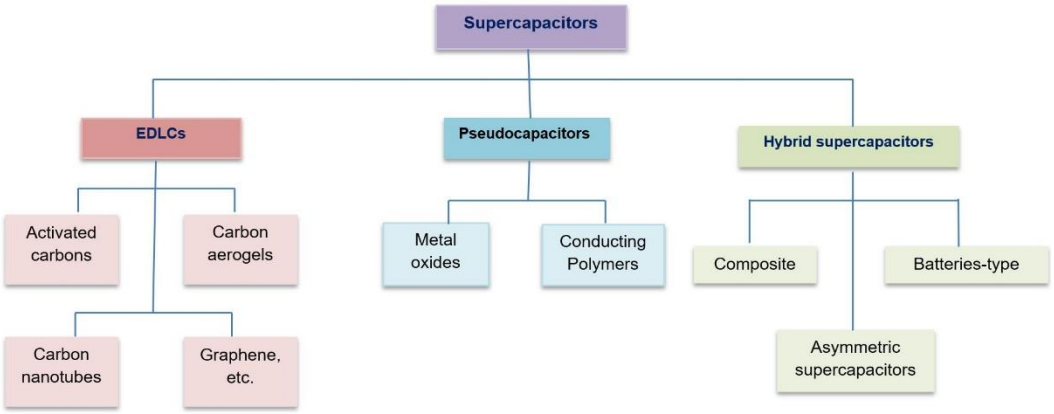

Fig.1-2. Typical classification of supercapacitors and related materials

In principle, pseudocapacitors offer high capacitance but they have low-cycle performance and rate capability is rather low while EDLCs provide relatively low capacitance but they can achieve rapid charge storage. Hybrid systems which combine positive features of both EDLCs and pseudocapacitors can be a more interesting choice that can achieve high power densities and energy in one device. Nonetheless, the performance of the device depends on the geometry, selection of electrolytes, fabrication of electrodes and properties of their active material [8, 12].

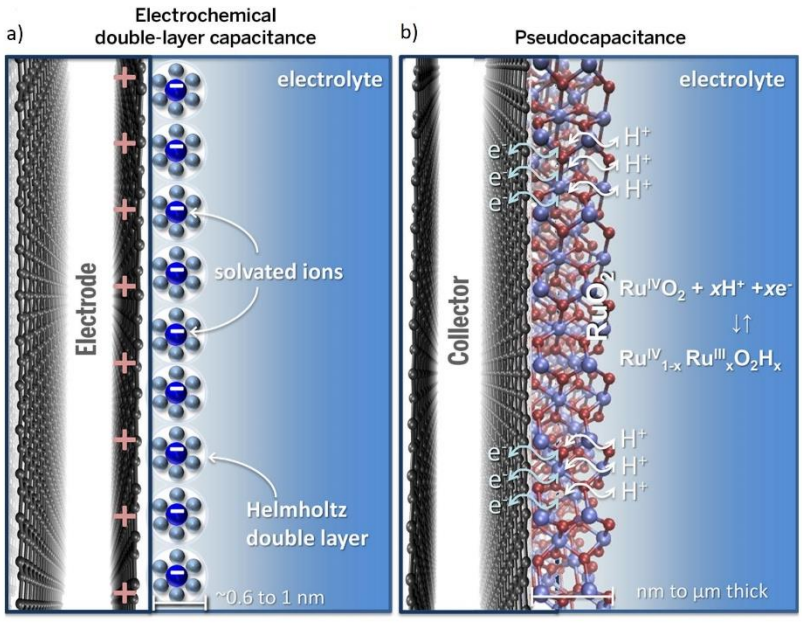

Fig.1-3. Scheme of charge storage in supercapacitors. a) Ion adsorption at the electrode surface (EDLC). b) Charge transfer near the surface of the electrode (pseudo-capacitance) [13].

1.2.2 Double Layer Capacitance

When two electrically charged layers are formed at the electrode/electrolyte interface, an electric double layer (EDL) is formed and it results in a potential-dependent charge storage ability.

The modeled concept of EDL was proposed by Helmholtz in the 19th century thus EDL is also referred to as Helmholtz double-layer. On the EDL model, at the interface of electrode/electrolyte two layers of opposite charges are formed and are separated in an atomic scale distance [14]. This model is similar to that of two-plate capacitors and as a result, the capacitance of EDL-based supercapacitors can be based on the simple model of two-plate capacitors:

Eq.1:

$$C = \frac{\varepsilon_r \varepsilon_0}{d} A$$

where ε_r is the electrolyte dielectric constant, ε_0 is the dielectric constant of the vacuum, d is the effective thickness of the double layer (charge separation distance) and A is the electrode surface area. However, the presence of the diffusion layer which forms due to the accumulation of ions close to the electrode surface is not considered in this equation.

Because of geometry constrains of the separation distance between the two charged plates and limited charge storage areas, according to this equation it is easy to see that conventional two-plate capacitors are only capable of storing a low energy amount. But the supercapacitors based on EDL, which normally use porous materials as their electrodes, store much more energy because of the high electrolyte/electrode interaction and the atomic scale of charge separation distances.

Later, the combined Gouy–Chapman-Stern model was established to more accurately describe the charge distribution of EDLs, by recognizing the inner Helmholtz plane (IHP, also referred to as compact layer or Stern layer) and outer Helmholtz plane (OHP, also referred to as diffuse layer) [14].

Depending on the used electrolyte, the double layer capacitance is between 5-20μF/cm^2[15]. Since organic electrolytes can sustain higher operation voltage (up to 2.7 V) they are more widely used although the achieved specific capacitance with aqueous alkaline or acid solutions is generally higher.

With organic electrolytes, the double layer capacitance of the activated carbon can reach 100-120 Fg^{-1} and at lower voltage it can even exceed 150-300 Fg^{-1} in aqueous electrolytes because the electrolyte voltage window is limited by water decomposition. A typical cyclic voltammogram of a

two electrode EDLC is presented in Fig.1-4. The rectangular shape is characteristic of pure double layer capacitance charge storage mechanism according to:

Eq.2:

$$I = C\frac{dv}{dt}$$

where I is the current C is the double layer capacitance and $\frac{dv}{dt}$ is the scan rate.

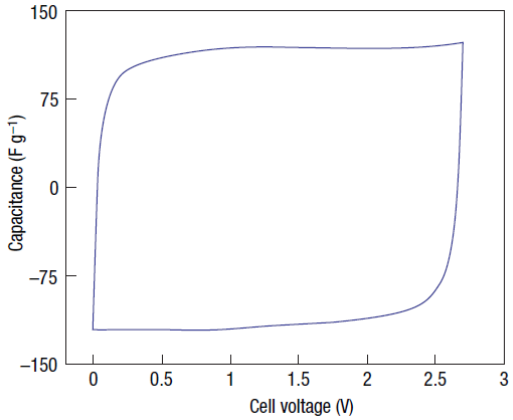

Fig.1-4. Cyclic voltammetry of a two-electrode laboratory EDLC cell [16]

According to:

Eq.3:

$$E = \frac{1}{2}CV^2$$

the stored energy is proportional to voltage squared. There is no redox (faradaic) reaction at the EDLC electrodes as a result of the electrostatic charge storage. There is no limitation by the electrochemical kinetics through a polarization resistance since a supercapacitor electrode is considered as a blocking electrode from and electrochemical point of view. In addition better power performance and very fast energy uptake and delivery are other results of this surface storage mechanism. The swelling in the active material which is observed in batteries during charge/discharge cycles is also eliminated due to the lack of faradic reactions. Batteries can survive a few thousand cycles whereas EDLCs can sustain millions. The solvent of the electrolyte is not involved in charge storage mechanism unlike Li-ion batteries where it contributes to the solid-electrolyte interphase when high potential cathodes or graphite anodes are used. The solvent choice is not limited because of this fact and different electrolytes with high performance at low temperature

can be designed for EDLCs. However, as a result of the electrostatic surface charging mechanism, EDLCs suffer from limited energy density.

1.2.3 Pseudocapacitance

Pseudo-capacitive behavior is defined as the use of fast reversible redox reactions at the surface/near surface of electrode materials. Compared with EDLC, pseudo-capacitance originates from thermodynamic reasons. The involved charge flow across the EDLs results in a faradaic current through the SC electrode. Such a faradaic charge transfer process results in an additional potential-dependent charge accumulation (charging) or release (discharging) behavior, the corresponding dQ/dv is equivalent to a capacitance, which is defined as the pseudo-capacitance.

There are mainly three types of faradaic processes for pseudo-capacitive electrodes: (1) reversible adsorption (such as adsorption-desorption of hydrogen on the surface of platinum or gold); (2) redox reactions of transition metal oxides (e.g. ruthenium oxide, manganese oxide, and vanadium nitride) [17, 18], and (3) reversible electrochemical doping/dedoping in electrically conductive polymers (e.g. polyaniline and polypyrrole) [19].

One major advantage of such faradaic electrochemical processes is that they can readily occur both on the surface and in the bulk near the surface of the electrode materials. Thus SCs based on pseudo-capacitance exhibit capacitance and energy density values 10-100 times larger than SCs based on EDLC, as reported by Conway et al. However, SCs based on pseudo-capacitance suffers from lower power densities, since faradaic processes are normally slower than non-faradaic processes. Moreover, the limited stability issue during cycling is also challenging.

Above all, for both charge storage mechanisms of EDLC and pseudo-capacitance, large surface area, appropriate pore-size distribution, and high conductivity are essential requirements for the electrode materials to achieve better electrochemical performance.

1.2.4 Hybrid Systems

Hybrid materials use an energy source (battery-like electrode) with a power source (capacitor-like electrode) in the same cell, offering an alternative to conventional pseudocapacitors or EDLCs. Cell voltage increase may even happen by using the appropriate electrode combination.

One of the approaches to achieve hybrid system is the use of pseudo-capacitive metal oxide with a capacitive carbon electrode (Fig.1-5).

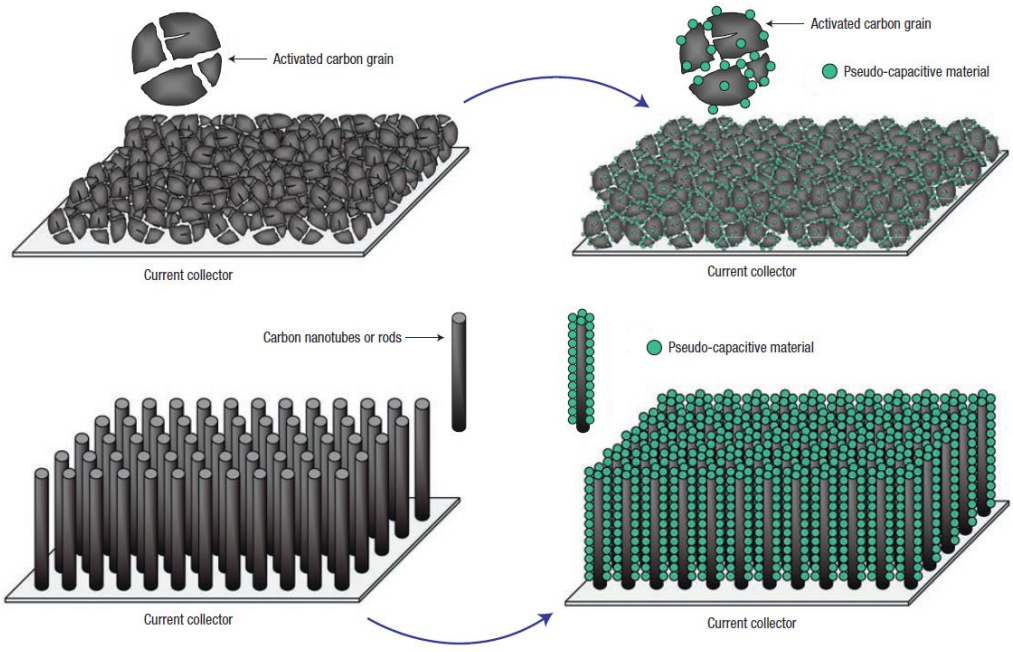

Fig.1-5. Decorating activated carbon grains (a) with pseudo-capacitive materials [16]

1.2.5 Micro-Supercapacitors

MSCs are high power microelectrochemical energy storage devices that were recently developed [20]. Recent progress in micro-fabrication technology has made it possible to produce micro-supercapacitors in an interdigitated planar from. This possibility contrasts with the conventional sandwich structure which is incompatible with integrated circuits.

MSCs are currently mainly used in electronic and on-chip applications that can directly be associated with energy-storage units, energy harvesting micro systems, microelectrochemical systems, and power supplies for electronic devices, powering micro-sensors, active radio frequency identification tags and biomedical implants [9, 20-23].

1.2.6 Micro-supercapacitors Production

Planar MSCs have attracted great attention due to the rapid progress of flexible, ultrathin miniaturized electronics. The key feature to use planar MSCs is to make the entire device smaller, more flexible and thinner in comparison with conventional supercapacitors with stack geometry. In the narrow space between electrode fingers, the electrolyte ions can transport rapidly and due to short

ion diffusion distance, they offer very high power capability. The separator which is used in conventional stacked supercapacitors is not needed in MSCs and this opens up the opportunity to produce MSCs with different thicknesses for different types of electronic applications (Fig.1-6). One of the main problems with the stack geometry is that it prohibits the transport of solid or gel-type electrolytes and as a result a big loss of power will occur. In particular, integration of the conventional supercapacitors into electronics is challenging due to the requirement of several steps for patterning the layers of current collectors, electrolyte and active materials and establishment of electrical connections at the ends [24].

MSCs have the benefit of easy fabrication of electronically isolated electrodes and the ability to be integrated into the miniaturized electronics on the same plane. Also, all types of electrolytes are suitable to be used and, finally, the easy adjustment of electrodes micropatterns leads to the reduction of internal impedance by minimizing the distance between adjacent interdigital electrodes.

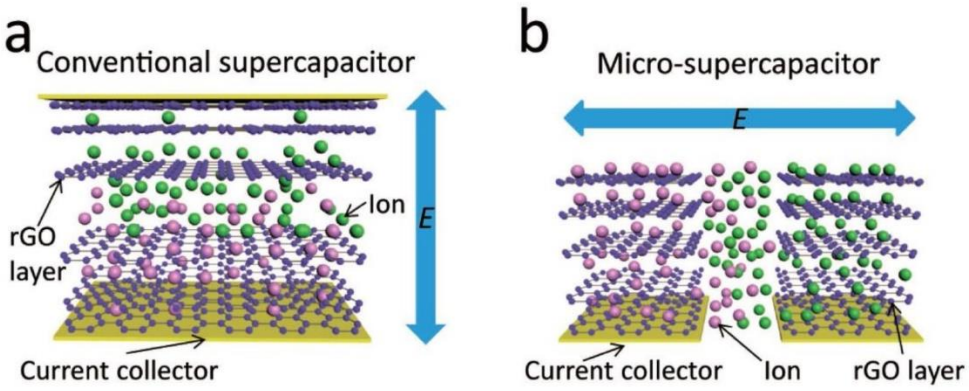

Fig.1-6. Schematic depiction of the operating principle of: a) the stacked-geometry conventional supercapacitors, and b) in-plane micro-supercapacitors [25]

1.2.7 Fabrication Materials

Using nanostructured electrochemically active materials, many efforts have been made in order to produce high power MSCs. Different types of materials have been used such as: carbide derived carbon, onion like carbon, and polyaniline [26] and polypyrrole [27], which belong to conducting polymers family with pseudocapacitance [21, 28]. In addition, transition metal oxides including ruthenium oxide [29] and manganese oxide [30] have been employed for production of MSCs. However, form materials perspective, carbon is inexpensive and earth abundant and as a

result various carbon nanomaterials have been employed for supercapacitor applications, either as the electrodes themselves or as the electrode substrate for future structure functionalization [2, 31].

Graphene, a sheet of sp^2 hybridized carbon atoms arranged in a honeycomb network, has been one of the most interesting topics of research since its discovery. It can be considered as the basic building block of all graphitic materials (Fig.1-7), it can be wrapped up into 0D fullerenes, rolled into 1D nanotubes or stacked into 3D graphite [32]. Graphene can be produced via different methods including: chemical exfoliation, electrochemical exfoliation [33], chemical vapor deposition [34], micromechanical cleavage [35] and by bottom up organic synthesis [36].

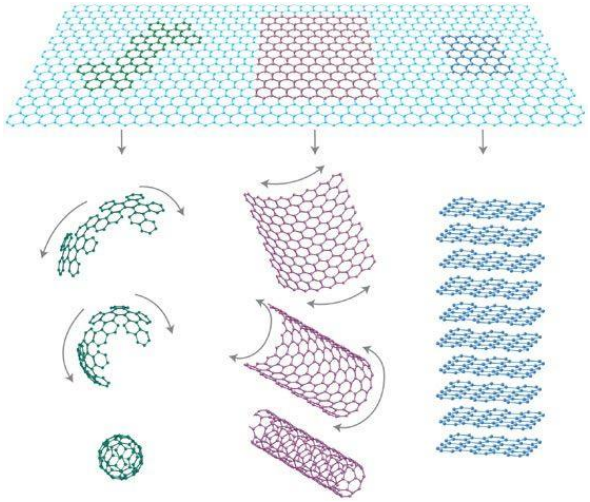

Fig.1-7. Graphene the basic building block of all graphitic materials[32]

The major possible uses of graphene in the near future include polymer hybrids, electronics, transparent conducting electrodes, batteries and supercapacitors [37]. Because of their excellent conductivity, high theoretical capacitance (~550 Fg^{-1}), high surface area (~2620 m^2g^{-1}) and exceptional intrinsic double-layer capacitance (~21μFcm^{-2}), graphene-based materials present a class of promising electrode materials for supercapacitors. Especially, planar MSCs based on graphene are superior to the conventional ones because they give the electrolyte ions the ability to interact with all graphene layers as demonstrated in Fig. 1-8 [38].

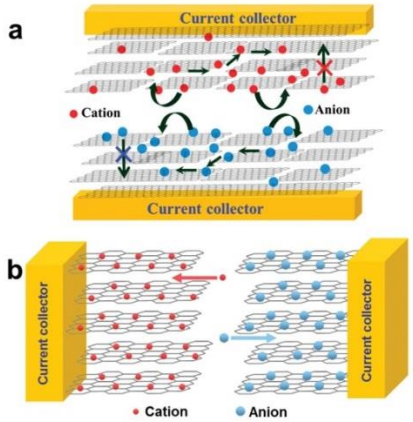

Fig.1-8. a) Conventional supercapacitors with stack geometry b) Operating principle of the in-plane supercapacitor device utilized for the performance evaluation of graphene as electrodes [38]

Using electronically conducting electrodes with high surface area is the key to reach high capacitance by charging the double layer. There are several candidates for this matter such as: carbon fabrics, activated, templated and carbide-derived carbons, nanotubes, fibers, nanohorns, onions and also graphitic carbon which can satisfy all the requirements for applications such as electrochemical stability, high conductivity and open porosity[15]. Because of their moderate cost and high surface area, activated carbons are the most used materials today. With heat treatment (carbonization) of a carbon reach organic precursors in inert atmosphere followed by selective oxidation in water vapor, KOH or CO_2, to increase the pore volume and the surface area, activated carbons are produced from carbon-rich organic materials. Both synthetic materials (polymers) and natural materials such as pitch, coal or wood can be used as precursors and the longer the activation time, the larger the mean pore size. Micropores (<2nm), mesopores (2-50 nm) and macropores (>50 nm) can be achieved as a porous network in the bulk of the carbon particles.

According to the energy formula of supercapacitor (Eq. 3), the energy density in the supercapacitor could be enhanced by increasing the voltage range or improving the specific capacitance. However, the voltage range is dependent on the electrochemical window of the electrode material and the stability potential window of the electrolytes. Compared to carbon-based materials, conductive polymers possess higher specific capacitance but their electrochemical window is very narrow.

Poly (3,4-ethylenedioxythiophene):poly (styrenesulfonate) (PEDOT:PSS) (chemical structure shown in Fig.1-9 is well-known for being one of the most promising conductive polymers due to the properties such as: high transparency, highly stable conductivity, chemical structural stability, fast and stable redox and good solubility in water. In addition, it possess a strong film forming ability

which is a big advantage to bring about large scale products by simple spraying, coating or printing techniques. These have been applied in different fields, e.g. liquid crystal displays, touchscreens, organic photovoltaics and light-emitting diodes[39].

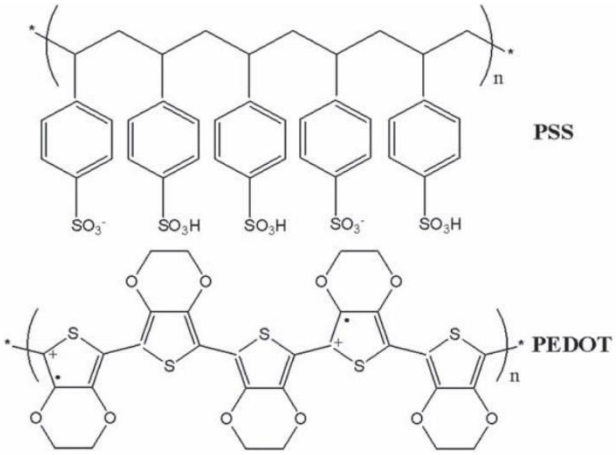

Fig. 1-9. Chemical structure of PEDOT:PSS

Ruthenium dioxide (RuO_2) is a very important material due to its unique qualities such as high thermal and chemical stability, metallic conductivity, field emitting behavior and electrochemical redox properties. RuO_2 applications in electronics include: integrated circuits, thick or thin film resistors, buffer layer for the high-temperature superconducting thin film, and ferroelectric films. In energy storage devices, in PtRU anodes of direct methanol fuel cells, ruthenium oxide is used to remove CO-like poisoning [40].

One of the good examples of good pseudo-capacitive materials is hydrous ruthenium oxide which can transfer between different oxidation states (Ru(IV)/Ru(III) and Ru(III)/Ru(II)) during redox reactions. The surface regions of RuO_2, while charging, are reduced to lower oxidation states at the same time with adsorption/insertion of hydrogen cations from the electrolyte. This process can be almost fully reversed during discharge. This whole process can be presented in the equation below [41]:

Eq.4:

$$RuO_x(OH)_y + \delta H^+ + \delta e^- \Leftrightarrow RuO_{x-\delta}(OH)_{y+\delta}$$

Chapter 2

Experimental Procedure

2.1 PEDOTT: PSS Device

For the preparation of the PEDOTT:PSS device the purchased polymer was Clevios PH1000 from Heraeus Clevios GmbH.

2.1.1 Porous Carbon Spheres Production

The mesoporous carbon powder was provided by a partner research group however the synthesis method is summarized in the following.

The mesoporous carbon spheres were prepared in two steps: firstly, by co-assembly of colloidal nanoparticles of silica with polyaniline (PANI), uniform SiO_2@PANI composite spheres were fabricated, as demonstrated in Fig.2-1. Secondly, mesoporous carbon spheres with high surface area, well-defined open pores and large pore volume were fabricated after carbonization and elimination of sacrificial SiO_2 template.

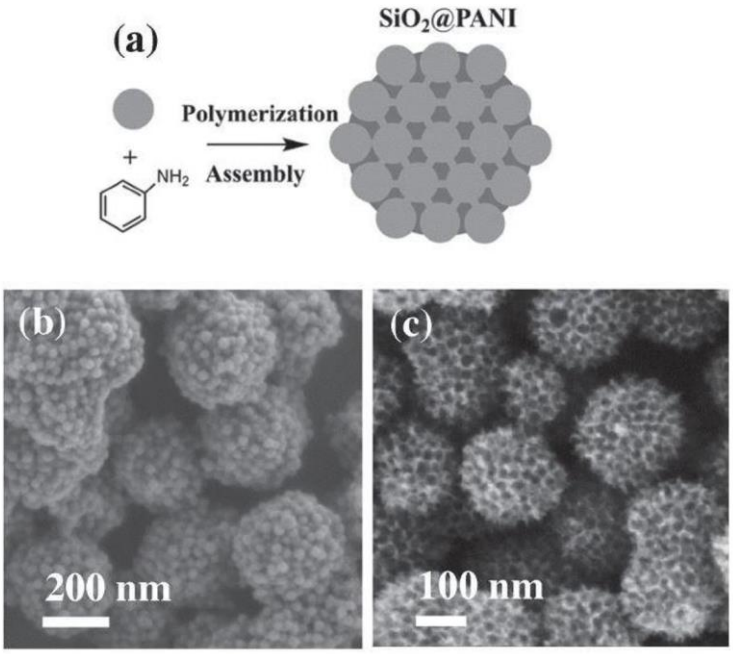

Fig.2-1. a) The formation process of MCS@MnO_2 spheres. SEM images of b) SiO_2@PANI c) MCSs [42].

2.1.2 Device Fabrication Procedure

In the first step of the device fabrication, a SiO_2 plate was cut into approximately 3×3 cm^2 squares and cleaned by sonication in ethanol, acetone and propan-2-ol each for 20 minutes. Porous carbon was added to PH1000 and sonicated for two hours. Since the powder was not dispersed well enough it was stirred overnight and sonicated for two more hours. Spin-coating was used for deposition of PH1000, and because of the hydrophilic nature of the PSS chain, O_2 plasma cleaning was undertaken on the substrates for 20 minutes to make it hydrophilic.

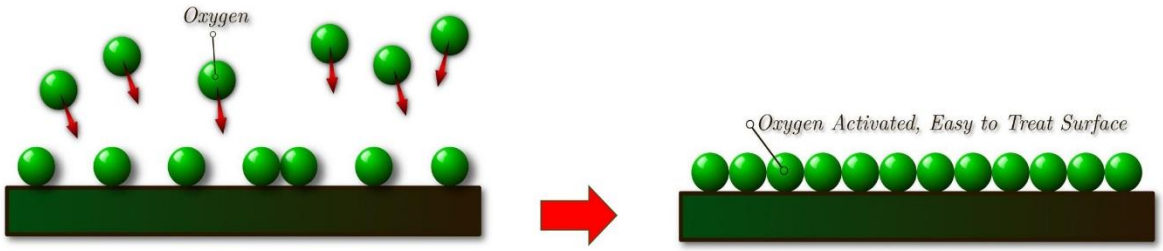

Fig.2-2. Plasma Cleaning

For the first series of samples no additional material was added to PH1000. 1 ml of PH1000 was measured and drop in a glass vial for each SiO_2 substrate. On each of two SiO_2 substrates PH1000 was dropped followed by spin-coating at 800 rpm. Then the samples were put in an oven with 150℃ for an hour to dry out, Fig.2-3.

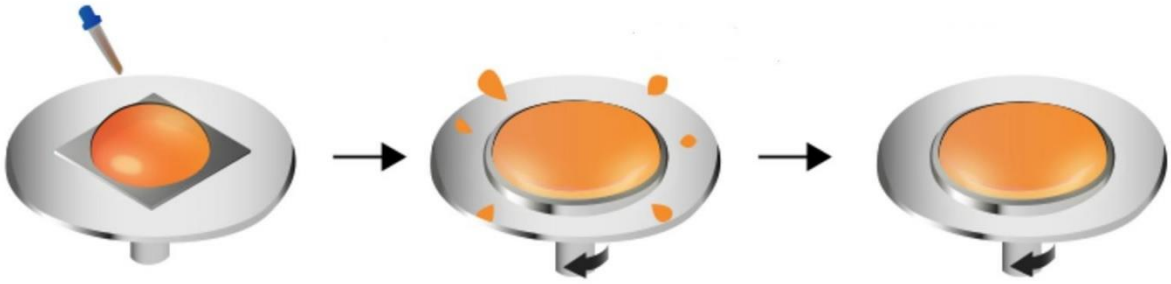

Fig.2-3. Spin coating process [1]

In the next step, one of the samples (sample 1-0) was put in concentrated sulfuric acid overnight and the next one (sample 1-1) was taken for gold deposition.

[1] www.spincoating.com

Afterwards, the gold collector was deposited on the polymer-covered SiO_2 substrate. For this step, a homemade shadow mask was used for the deposition of gold and current collectors were used. For each device, two steps of deposition were performed as the masks were separated into two different parts. After completing the deposition step each sample's thickness was measured by a profilometer (Fig. 2-4) followed by oxidative etching of MSC channels in oxygen plasma. Then, the thickness was measured again (Fig2-5) to find-out the real thickness of the electrode.

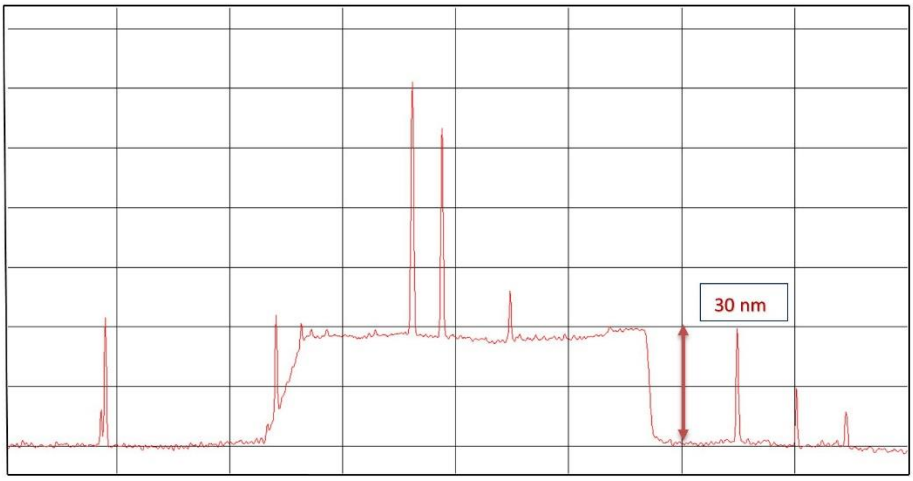

Fig.2-4. Sample thickness measured by the profiler before plasma etching

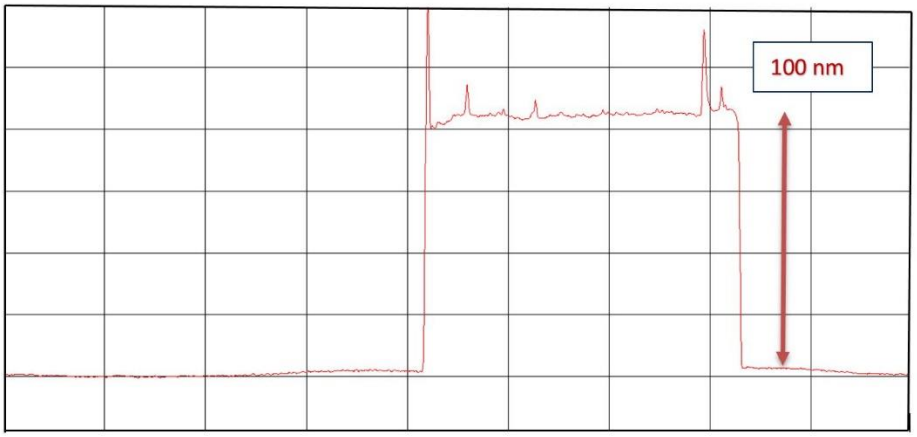

Fig.2-5. Sample thickness measured by the profiler after plasma etching

For the next devices, porous carbon powder was added to the PH1000. Different amounts of porous carbon were measured to produce hybrid inks with different ratios. After each measurement, the powder was added to the polymer and the mixture was sonicated for 2 hours followed by

overnight stirring. The following steps were performed as explained before. In the table below, the sample ratios and their code are summarized.

Table 2-1. Summary of the sample codes for PH000/Porous Carbon Hybrid Ink

Code	PH1000 (%)	Porous Carbon (%)	Acid Treatment
1-0	100	0	No
1-1	100	0	Yes
1-2	90	10	Yes
1-3	75	25	Yes
1-4	50	50	Yes

Subsequently, a gel electrolyte of poly vinyl alcohol (PVA)/H_2SO_4 was drop-casted onto the finger electrodes and allowed to solidify overnight yielding the in-plane structured MSC (the process is depicted in Fig.2-6). The cupper foils were attached to the electrode using a silver paste and finally the electrochemical behavior of on-chip planar MSCs based on PH1000 porous carbon was studied by cyclic voltammetry (CV).

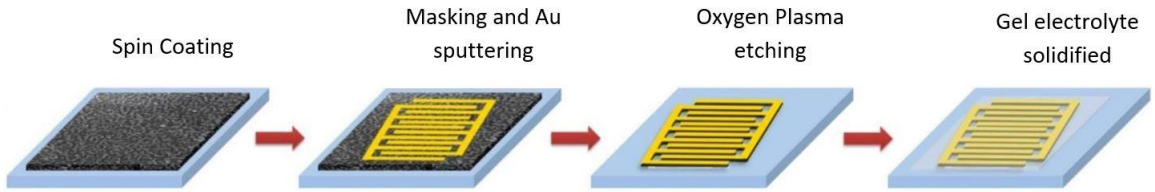

Fig.2-6. Schematic illustration of fabrication process of the MSC devices

The device fabrication steps are summarized in the flow chart shown in Fig.2-7.

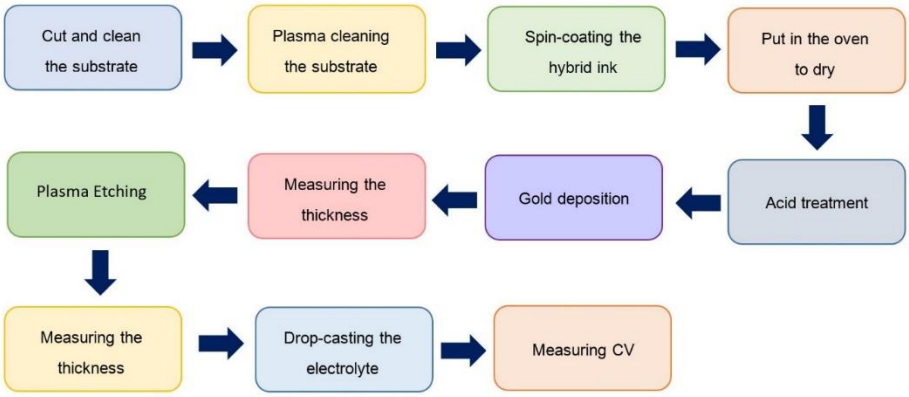

Fig.2-7. Summary of the device fabrication process

2.2 EG/RuO_2 Hybrid System

Recently, electrochemical exfoliation of graphite has attracted much attention due to its easy, fast, and environmentally friendly nature to produce high-quality graphene in bulk scale [43, 44]. However, due to the lack of abundant functional groups on the surface, electrochemically exfoliated graphene (EG) can only be dispersed in high boiling point solvents like N-methyl-2-pyrrolidone (NMP) or N,N'-dimethylformamide (DMF). This makes difficult to employ conventional solution processing techniques for thin film preparation, such as spin-coating, inkjet-printing, rod-coating and/or layer-by-layer deposition[45].

2.2.1 EG Production

EG was produced as previously reported by the host group of the present internship [43]. In summary, a home-built set up (Fig.2.8a) was used for the electrochemical process. Basically, a voltage was applied between the two electrodes to drive structural expansion and subsequent exfoliation at the graphite side. Graphene was produced by exfoliation of a rolled-up graphite foil which was used as electrode. The graphite foil was pretreated with liquid nitrogen and ethanol which resulted in volume expansion, assisting the exfoliation process. Sulfuric acid (0.1M solution) was used as the electrolyte and platinum as the counter electrode. The graphite anodes were detached into small pieces and spread into the solution where a positive voltage of 10V was applied. This bias voltage was kept constant for approximately 2 minutes to complete the exfoliation process (Fig.2-8b). Afterwards, the resulting graphene products were collected by vacuum filtration and washed

with water for several times to remove the residual acid. Finally, the obtained powder was dispersed in Dimethylformamide (DMF).

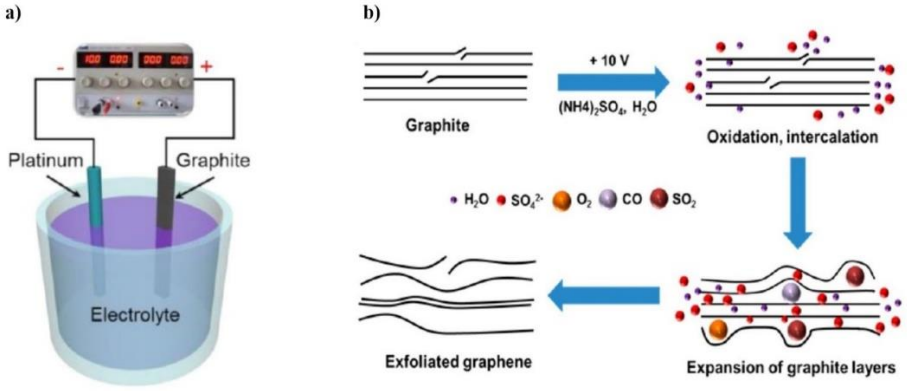

Fig.2-8, a) Setup for electrochemical exfoliation. b) Schematic illustration of the mechanism of electrochemical exfoliation of graphite[43].

2.2.2 RuO_2 Production

RuO2 was given by a research partner group however the preparation method is described in the following.

Exfoliation of layered $Na_{0.2}RuO_2$ resulted in suspension of layered RuO_2 nanosheets. First, the layered $Na_{0.2}RuO_2$ was produced by a treatment of $NaRuO_2$ with $Na_2S_2O_8$ solution to remove the excess Na ions. Then, $Na_{0.2}RuO_2$ was protonated by a reacting it with 1 M HCL solution. The protonated products were put in reaction with tetrabutylammonium (TBA^+) ions for more than 10 days yielding RuO_2 nanosheets [46].

2.2.3 Device Fabrication Procedure

Since the EG was dispersed in DMF and it is hydrophobic, it was not possible to use spin coating as a method for production of these samples. Instead vacuum filtration was used and a home-made set-up was employed for transferring the graphene/RuO_2 layer to the substrate.

The EG solution concentration was 100 mg in 80 ml, starting with 2 ml of the solution and obtaining as a result 2.5 mg of EG. For the first sample, 2.5 mg of RuO_2 was weighted to prepare a 50-50 ratio of the hybrid ink. Since dispersing RuO_2 in the EG solution was challenging, 28 ml of DMF was added to the mixture and sonicated until any agglomeration was seen. Next different

concentrations from this sample were prepared: 2, 4, 6 and 8 ml of this mixture were added to 28, 26, 24 and 22 ml of DMF, respectively, and sonicated for two more hours.

In the following step, vacuum filtration with PTFE membranes was undertaken. This process had to be done in a clean room but since there was no access to a clean room, avoiding dust and contamination was challenging. The whole process is self-regulating, which allows fine control over the graphene film thickness by varying the concentration or volume of EG dispersion. This method can be applied to both rigid and flexible substrates. After filtering each solution, the membrane was put on top of the SiO_2 substrate and then they were inserted between two plates and kept under pressure using our home-made set-up for more than 12 hours (depending on the concentration of the ink). This step is illustrated in Fig.2-9.

Fig.2-9. Transferring procedure: a) vacuum filtration, b) home-made set-up

In the next step, the membrane was removed and if the EG layer was transferred properly to the substrate, it was heated at 180℃ in an oven for one hour to remove the DMF residuals. The following steps were similar to the first part: deposition of Au collectors, plasma etching and drop casting the gel electrolyte. As the device was kept for deposition of the gold collectors 100 nm was a chosen for the gold layer (Fig.2-10).

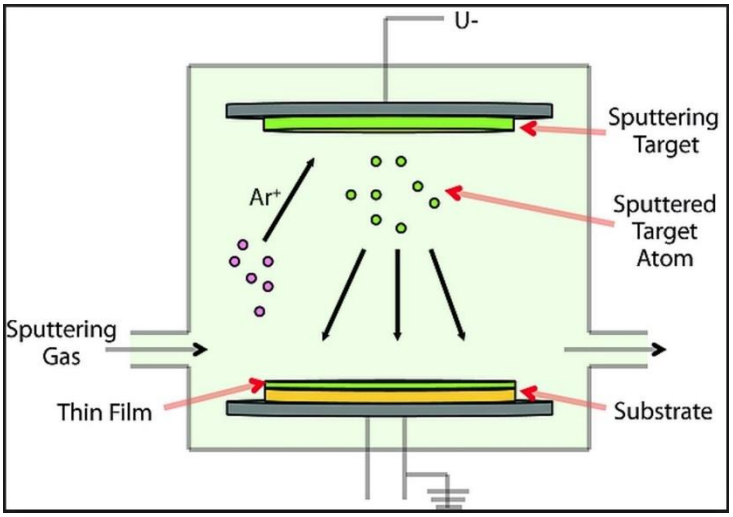

Fig.2-10. Schematic illustration of gold deposition

After gold deposition, oxygen plasma was used to etch the sample. This step of the process was the most difficult since the sample was very sensitive to oxygen plasma and the etching process had to be done on several steps and sometimes it damaged the gold collectors (Fig.2-11). The thicker the sample was, the more difficult the etching step became as it could oxygen atoms could easily ruin the device because of the instability of the gold layer on top of a thick layer of hybrid ink.

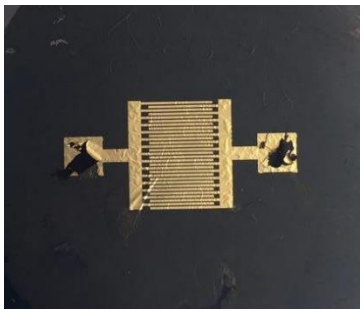

Fig.2-11, Failed etching process

PVA/H_2SO_4 gel was used also here as the electrolyte, it was drop-casted on the gold collectors and the copper wires were attached to each side of the MSC using silver paste. After waiting overnight in order to let the electrolyte solidify, the device was ready for CV measurements. Harmful leakage of liquid electrolyte was avoided by using this gel type of electrolyte and also it was useful for reducing the micro device thickness without additional packaging materials.

Different ratios and concentrations of EG/RuO_2 hybrid ink in DMF were prepared which are summarized in Table 2-2.

Table 2-2. Summary of the sample codes for EG/RuO_2 hybrid ink

Code	**EG (ratio)**	**RuO_2 (ratio)**	**Concentration (ml)**
2-0	1	0	_
2-1	1	1	2
2-2	1	1	4
2-3	1	1	6
2-4	3	1	2
2-5	3	1	4
2-6	3	1	6

Chapter 3

Characterization Methods

Several characterization methods have been used in this work including cyclic voltammetry, scanning electron microscopy (SEM), atomic force microscopy (AFM) and x-ray diffraction. A summary of these characterization methods is given in this chapter.

3.1 Cyclic Voltammetry figure of merits

Cyclic voltammetry (CV), galvanostatic charge/discharge (GCD), and electrochemical impedance spectroscopy (EIS) measurements are commonly used to evaluate the performance of a supercapacitor.

In principle, there are three fundamental parameters: voltage (V), current (I), and time (t). Physical quantities, including the capacitance (C), energy (E) and power (P) densities, operating voltage (V_O) and equivalent series resistance (R_{ES}) of the SC can be calculated from them.

When addressing the total charge storage ability of a SC device, the total capacitance C_T of a SC is a calculated by the stored electrical charge ΔQ under a given voltage change ΔV:

Eq.5:

$$C_T = \Delta Q / \Delta V$$

Generally, a more intrinsic specific capacitance C_S is employed to demonstrate the charge storage ability of SC materials:

Eq.6:

$$C_S = \Delta Q / \Delta V \Pi$$

where Π can be the mass, surface area and volume of the SC electrode material, and the result in specific capacitance C_S is often named correspondingly as the gravimetric capacitance ($F.g^{-1}$), areal capacitance ($F.cm^{-2}$), and volumetric capacitance ($F.cm^{-3}$).

The MSC device capacitance (C_{device}) values can be calculated from the CV curves according to the following equation:

Eq.7:

$$C_{device} = \frac{1}{\nu(V_f - V_i)} \int_{V_i}^{V_f} I(V)dV$$

where ν is the scan rate, V_f and V*i* are the integration potential limits of the CV curve. I(V) is the voltammetric discharge current. Specific areal (C_{areal}) and volumetric capacitance ($C_{volumetric}$) were calculated according to:

Eq.8:

$$C_{areal} = C_{device}/A$$

where A is the total area of the device.

Eq.9:

$$C_{volumetric} = C_{device}/V$$

where V is the total volume of the device.

As for GCD tests, a constant current is used, thus C_T calculation can be expressed as:

Eq.10:

$$C_T = I * \Delta t/\Delta V$$

where I is the constant discharge current, Δt is the discharge time, ΔV is the voltage change.

The energy density of a MSC device can be calculated as:

Eq.11:

$$E = \frac{1}{2} \times C_{volumetric} \times \frac{(\Delta V)^2}{3600}$$

where E is the energy density (in $W.h.cm^{-3}$), ΔV is the discharge voltage range.

The power density of the MSC device can be calculated as:

Eq.12:

$$P = \frac{E}{\Delta t} \times 3600$$

where P is the power density (in $W.cm^{-3}$) and Δt the discharge time (in seconds).

The operating voltage V_O is defined as the potential applied to the electrochemical system or the suitable potential window within which a SC device is normally operated. Both the solvent of electrolytes and cell configuration determines the V_O. In an aqueous system, V_O is normally 1 V due to the decomposition potential of water, while based on organic electrolyte, the V_O varies between 2.3 to 2.7 V. In an aqueous system based on an asymmetric configuration, V_O can be increased to 2.0-2.3 V by employing different SC electrode materials.

A SC has its own internal resistance, which can be regarded as an equal RC circuit: a capacitor connected in series with a resistor. That is how the equivalent series resistance (R_{ES}) is defined. R_{ES} is normally evaluated through the analysis of the IR drop or voltage variation at the initial stage of the discharging curve from GCD tests. By applying Ohm's law to the IR drop, R_{ES} can be obtained readily:

Eq.13:

$$R_{ES} = \Delta V / \Delta I$$

where ΔV and ΔI are the voltage and current of the IR drop, respectively.

3.2 Atomic Force Microscopy

Atomic force microscopy is a type of scanning probe microscopy which consist of a cantilever with a sharp nanoscale tip which scans the surface of the sample and operates based on the interaction forces between the tip and the specimen (Fig.3-1).

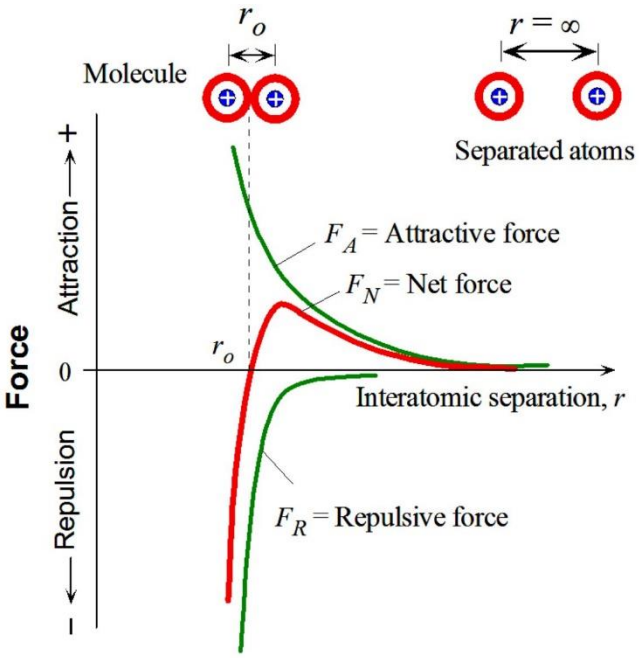

Fig.3-1. Qualitative behavior of the force between tip and sample as function of tip-sample distance [1]

Using the deflection from the cantilever on which the tip is mounted, the force between tip and sample can be measured. The cantilever deflection is proportional to the tip-sample force as it acts as a spring. The movement of the cantilever is detected using a laser beam which will be deflected according to the cantilever and give information about the topography of the sample. The tip can move precisely across the sample using piezoelectric effect (Fig.3-2).

[1] www.doitpoms.ac.uk/tlplib/afm/tip_surface_interaction

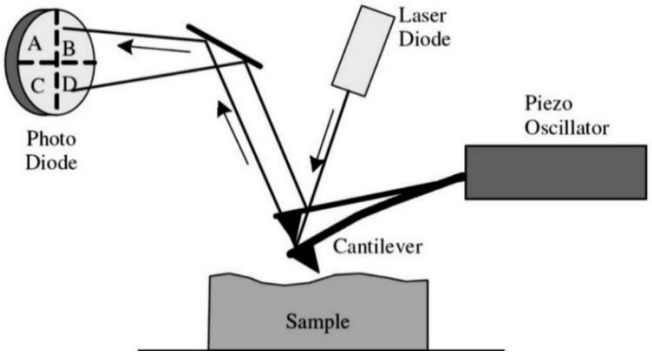

Fig.3-2. Schematics of atomic force microscopy operation [48]

Mainly, there are three operation modes described for AFM: (1) contact mode; (2) non-contact mode; and (3) intermittent contact mode or tapping mode. As it can be read from the designation, in contact mode the tip is in a continuous contact with the sample and the signals arise from the height difference in the sample during and the force is constant during the time of the measurement. This mode has the disadvantage of damaging the tip because of the contact with the sample. In contrast, in non-contact mode the height is constant and the force is varying. In this mode the signal comes from the amplitude or resonance frequency modulation due to the interaction of the tip with the sample. Finally, in the tapping mode, the tip comes into intermittent contact with the sample leading to a short-range force contributions close to the sample which changes the oscillation amplitude. A constant driving frequency very close to the resonance of the free cantilever is usually used in this mode. Non-contact and tapping mode are preferred for soft samples. Here tapping mode was used by dimension icon equipment by Bruker.

3.3 Scanning Electron Microscopy

Scanning electron microscopy is one type of electron microscopy which uses the electron beam to scan the sample in order to resolve topographical features of the sample and providing atomic number difference over the sample.

When the electron beam reaches the sample, several types of interaction might happen. In Fig.3-3 the interaction volume for various scattering types are illustrated. Topological features of the sample can be seen when secondary electrons are emitted in photoemission mode of SEM. When the electrons are scattered elastically and dependent on the atomic number of the target atoms, they are called backscattered electrons and they reveal information about the composition of the sample.

Backscatter mode is useful for realizing different phases and precipitates in the microstructure of the sample and does not require the sample to be etched.

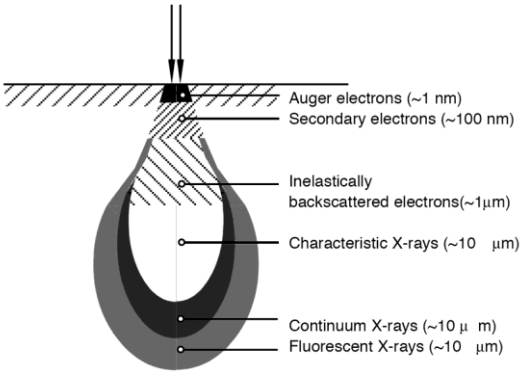

Fig.3-3. Interaction volume for various electron scattering types in SEM [49]

By collecting the characteristic x-rays emitted from excited atoms, quantitative analysis of individual points is made possible and called energy dispersive x-ray spectroscopy (EDX). The working principle is based on the fact that each element produces an x-ray with a unique amount of energy which is then collected by EDX detector. EDX is efficient at detecting elements with atomic number greater than 9.

The SEM components in Fig.3-4 consist of:

- Electron Source ("Gun")
- Electron Lenses
- Sample Stage
- Detectors for all signals of interest
- Display / Data output devices
- Infrastructure Requirements:
- Power Supply
- Vacuum System
- Cooling system
- Vibration-free floor
- Room free of ambient magnetic and electric fields

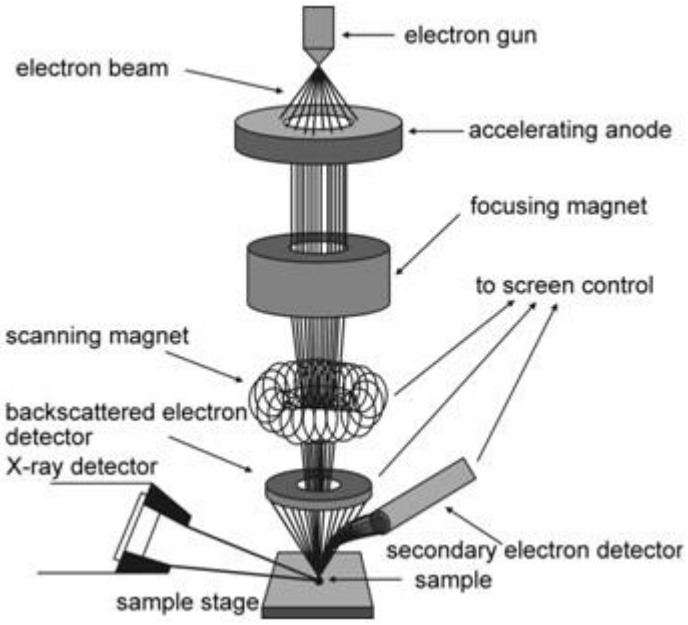

Fig.3-4. SEM set-up [1]

Secondary electrons energy is in the range of eV and they come from the electrons from depth of few nanometers on the surface of the sample and they can be detected using Everhart-Thornley detector or In Lense detector which are placed aside and above the sample respectively. By using BSE, the energy range is in keV area and images with increased material contrast can be obtained based on the fact that heavy elements backscatter more electrons that light elements and as a result they appear brighter on the image.

Because of the electrostatic interaction between the sample and the electron beam, electrical charging of the sample can lead to the movement of the sample which is not desirable and as a result, SEM samples are supposed to be conductive to avoid electrical charging. Insulating samples should be coated with a gold or carbon layer before imaging by sputter deposition [50]. Here HITACHI UHR FE-SEM SU8000 was used for SEM and Bruker X-Flash 5010 for EDX measurements.

[1] www.technoorg.hu/news-and-events/articles/high-resolution-scanning-electron-microscopy-1

3.4 X-Ray Diffraction (XRD)

XRD is the primary technique for characterizing compounds and obtaining information about their crystal structure, phase, texture (preferred crystal orientation) and other structural parameters such as crystal defects, strain, crystallinity and average grain size. The working principal of XRD, Fig. 3-5, is based on the dual nature of particle/wave of x-rays. When an incident beam of X-ray interacts with a target material, it scatters in a form of X-ray. Based on the crystal structure of the target sample, these scattered X-rays undergo constructive and destructive interference which is called "diffraction". Diffraction process is described by Bragg's law ($n\lambda=2d\sin\theta$) where n is a positive integer, λ is the wavelength of the incident wave, d is the interplanar distance of the crystal lattice and θ is the scattering angle [51].

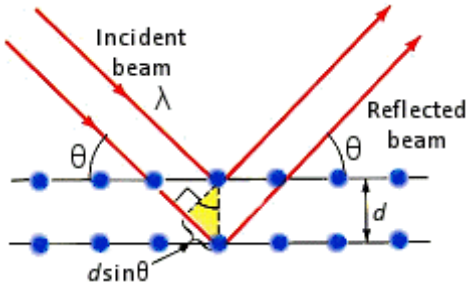

Fig.3-5. Schematic illustration of Bragg's law [52]

The unit cell's shape and size affects the direction of the diffracted beam and the intensity of the beam depends on the arrangement of the atoms in the crystal structure.

X-ray diffractometer consist of three main elements: an X-ray tube, a sample holder and an X-ray detector. A filament is heated in a cathode ray tube to produce electrons and as a result X-rays are generated. The material is bombarded with electrons which are accelerated toward the target by applying a voltage.

If the electrons have enough energy, they dislodge inner shell electrons of the target material and as a result characteristic X-ray spectra are produced. Monochromatic X-rays are needed for diffraction so monochrometers are used in the set-up. The most common components of the spectra are K_α and K_β. K_α consist of $K_{\alpha1}$ and $K_{\alpha2}$ where $K_{\alpha1}$ has twice the intensity and slightly shorter wavelength as $K_{\alpha2}$. Based on the target material's characteristic (Cu, Fe, Cr, Mo) the specific wavelengths changes. The most common target for single crystal diffraction is copper with CuK_α = 1.5418°A. These X-rays are modified and directed to the sample. The intensity of the X-rays is

recorded as the sample and detector are rotated. When the Bragg equation is satisfied by the impinging X-ray on the sample, constructive interference and as a result a peak in intensity occurs. These X-ray signals are recorded and processed by the detector and converted to a count rate which is then delivered to the output device such as a computer.

X-ray diffractometer geometry is such that the sample rotates at a θ angle in the path of the X-ray and the detector rotates at an angle of 2θ. Goniometer is the name of the equipment used to rotate the sample and maintain the angle. The data for typical powder patterns is collected from 2θ from five to seventy degrees. Here Guinier Imaging Plate Camera G670 from Huber Diffraktionstechnik was used.

Chapter 4

Results and Discussion

4.1 PEDOT:PSS/ Porous Carbon Hybrid Ink

Cyclic voltammetry was the first method used to study the device performance. As explained before, a PVA/H_2SO_4 gel was used as the electrolyte. Since this gel was drop-casted, any contact with the copper wires and the electrolyte resulted in a short-circuit and as a result, device failure. Here, we report the results from the cyclic voltammetry in the form of areal and volumetric capacitance.

For the devices based on PEDOT: PSS and porous carbon, first we measured the performance without addition of any porous carbon. Results are shown in Table 4-1.

Table 4-1, CV results from device 1-0

Scan Rate	Integral	Device Area(cm^2)	C_{area} ($\mu F/cm^2$)	Thickness (nm)	Volume (cm^3)	C_{volume} F/cm^3
0.01	7.49E-07	0.5	150	70	0.0000035	21.38
0.05	4.31E-06	0.5	173	70	0.0000035	24.64
0.1	9.28E-06	0.5	186	70	0.0000035	26.50
0.5	4.07E-05	0.5	163	70	0.0000035	23.23
1	7.59E-05	0.5	152	70	0.0000035	21.68
5	2.73E-04	0.5	109	70	0.0000035	15.57
10	4.60E-04	0.5	91.9	70	0.0000035	13.13
50	0.001288	0.5	51.5	70	0.0000035	7.36
100	0.00154	0.5	30.8	70	0.0000035	4.40
200	0.001602	0.5	16.0	70	0.0000035	2.28
1000	0.001786	0.5	3.57	70	0.0000035	0.51

Table 4-2, CV results from device 1-1

Scan Rate	Integral	Device Area(cm^2)	C_{area} ($\mu F/cm^2$)	Thickness (nm)	Volume (cm^3)	C_{volume} F/cm^3
0.01	9.51E-07	0.5	190	76	0.0000038	25.01
0.05	5.00E-06	0.5	200	76	0.0000038	26.31
0.1	1.06E-05	0.5	212	76	0.0000038	27.87
0.5	4.78E-05	0.5	191	76	0.0000038	25.14
1	9.17E-05	0.5	183	76	0.0000038	24.13
5	3.86E-04	0.5	154	76	0.0000038	20.31
10	6.44E-04	0.5	129	76	0.0000038	16.93
50	0.001671	0.5	66.9	76	0.0000038	8.79
100	0.001979	0.5	39.6	76	0.0000038	5.20
200	0.002057	0.5	20.6	76	0.0000038	2.70
1000	0.001984	0.5	3.97	76	0.0000038	0.52

As we expected and based on previous studies[53], the device which were treated with acid for 24 hours (sample 1-1), had better performance. During this treatment, the insulating PSS part of

the polymer were dissolved resulting in better conductivity. CV curves of the device 1-1 are illustrated in Fig.4-1.

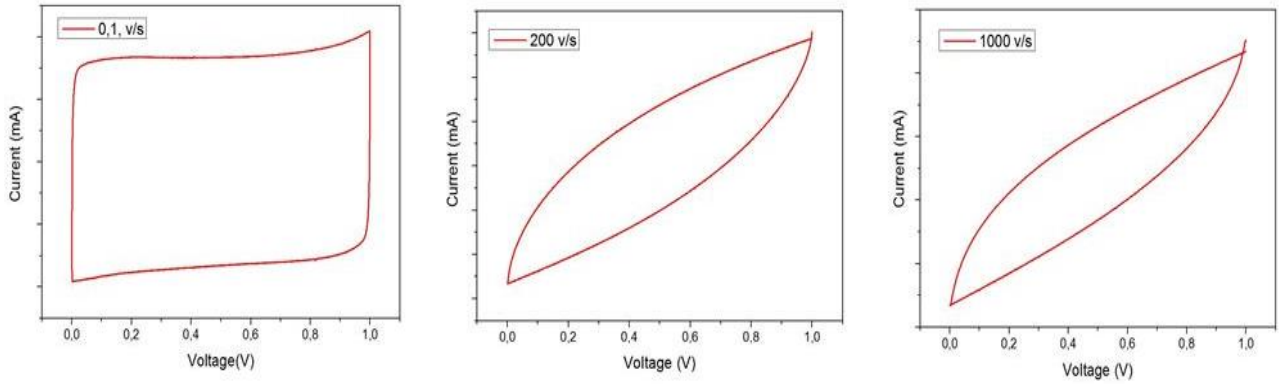

Fig.4-1, CV curves of device 1-1 in 0.1, 200 and 1000 V/s scan rates

A rectangular shape of the cyclic voltammogram proves a high charge storage EDL mechanismas with pseudo-capacitance mechanism. Although this means PH1000 has a good performance by its own, they suffer from limited stability during cycling which reduces the initial performance when used as a bulk material [4]. It can also be seen in the graph that with increasing the scan rate, the rectangular shape which has a direct relation with the capacitance is lost which confirms the lack of stability.

In the next step we added the porous carbon. The results from device 1-2 are illustrated in Tables 4-3 to 4-5 and the respective CV curves are given in Figs. 4-2 to 4-4.

Table 4-3, CV results from device 1-2

Scan Rate	Integral	Device Area(cm^2)	C_{area} (µF/cm2)	Thickness (nm)	Volume (cm^3)	C_{volume} F/cm^3
0.01	1.59E-07	0.5	31.9	55	0.00000275	5.79
0.05	8.31E-07	0.5	33.2	55	0.00000275	6.04
0.1	1.91E-06	0.5	38.3	55	0.00000275	6.96
0.5	7.91E-06	0.5	31.6	55	0.00000275	5.75
1	1.54E-05	0.5	30.7	55	0.00000275	5.58
5	6.92E-05	0.5	27.1	55	0.00000275	5.03
10	1.28E-04	0.5	25.6	55	0.00000275	4.65
50	4.53E-04	0.5	18.1	55	0.00000275	3.29
100	7.23E-04	0.5	14.5	55	0.00000275	2.62
200	0.001127	0.5	11.3	55	0.00000275	2.04
1000	0.002708	0.5	5.42	55	0.00000275	0.98

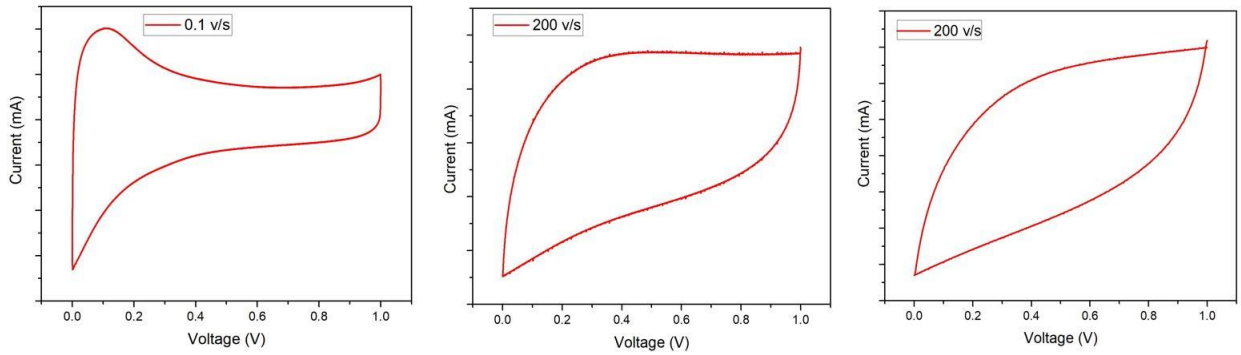

Fig.4-2, CV curves of device 1-2 in 0.1, 200 and 1000 V/s scan rates

Table 4-4, CV results from device 1-3

Scan Rate	Integral	Device Area(cm^2)	C_{area} ($\mu F/cm^2$)	Thickness (nm)	Volume (cm^3)	C_{volume} F/cm^3
0.01	5.98E-07	0.5	120	161	0.00000805	7.42
0.05	3.19E-06	0.5	128	161	0.00000805	7.92
0.1	6.35E-06	0.5	127	161	0.00000805	7.88
0.5	3.05E-05	0.5	122	161	0.00000805	7.56
1	5.93E-05	0.5	119	161	0.00000805	7.36
5	2.69E-04	0.5	107	161	0.00000805	6.67
10	4.99E-04	0.5	99.8	161	0.00000805	6.19
50	0.001636	0.5	65.4	161	0.00000805	4.06
100	0.002365	0.5	47.3	161	0.00000805	2.93
200	0.00311	0.5	31.1	161	0.00000805	1.93
1000	0.002171	0.5	4.34	161	0.00000805	0.26

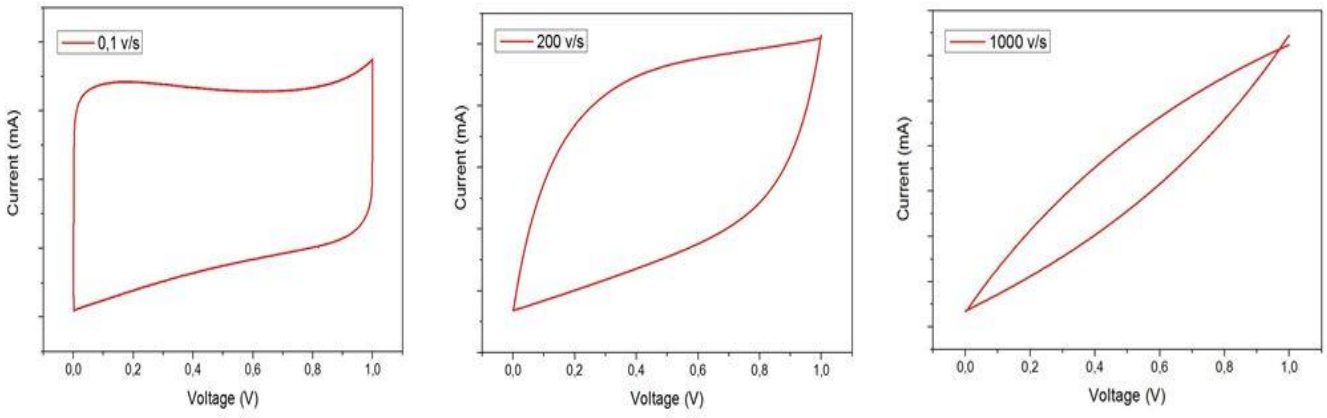

Fig.4-3, CV curves of device 1-3 in 0.1, 200 and 1000 V/s scan rates

Table 4-5, CV results from device 1-4

Scan Rate	Integral	Device Area(cm^2)	C_{area} ($\mu F/cm^2$)	Thickness (nm)	Volume (cm^3)	C_{volume} F/cm^3
0.01	1.02E-06	0.5	203	167	0.00000835	12.18
0.05	5.02E-06	0.5	201	167	0.00000835	12.02
0.1	9.78E-06	0.5	196	167	0.00000835	11.71
0.5	4.50E-05	0.5	180	167	0.00000835	10.78
1	8.57E-05	0.5	171	167	0.00000835	10.26
5	3.51E-04	0.5	141	167	0.00000835	8.41
10	5.87E-04	0.5	117	167	0.00000835	7.03
50	1.13E-03	0.5	45.2	167	0.00000835	2.70
100	1.07E-03	0.5	21.4	167	0.00000835	1.27
200	7.52E-04	0.5	7.52	167	0.00000835	0.45
1000	6.31E-05	0.5	1.26	167	0.00000835	0.0075

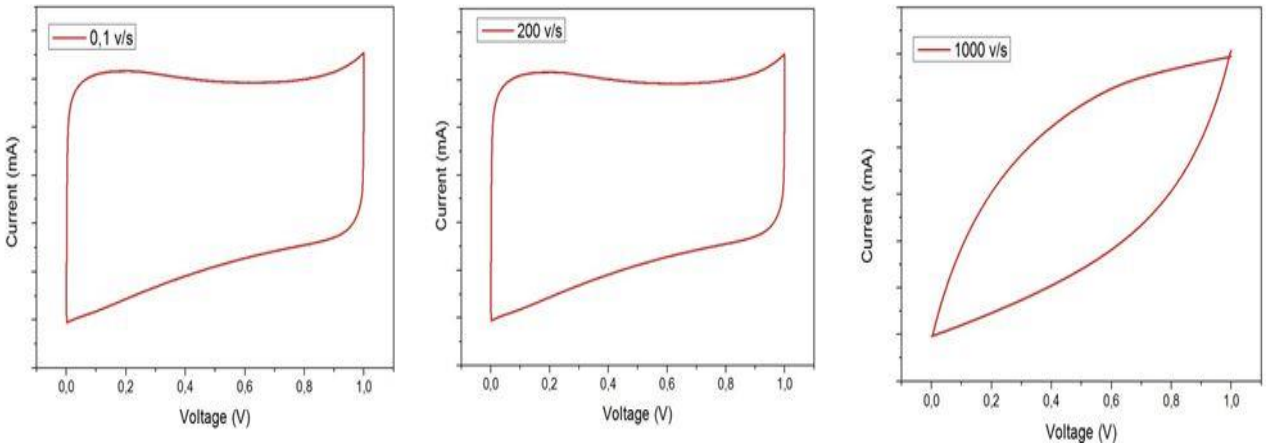

Fig.4-4, CV curves of device 1-4 in 0.1, 200 and 1000 V/s scan rates

Based on these results, the capacitance has actually decreased after the addition of porous carbon which was not expected. However, the quasi-rectangular shape even at ultra-high scan rates of 200 V/s reflects an ultrafast charge propagation and ion diffusion within the electrodes as well as the indicative of existence of electrical double-layer[23]. This was expected because of the high specific area of the porous carbon that should be able to enhance the capacitance by using electrochemical double-layer charge storage as an additional mechanism. Also, better stability was expected from the new hybrid material which is shown when the "capacitance retention" is calculated (Fig.4-5).

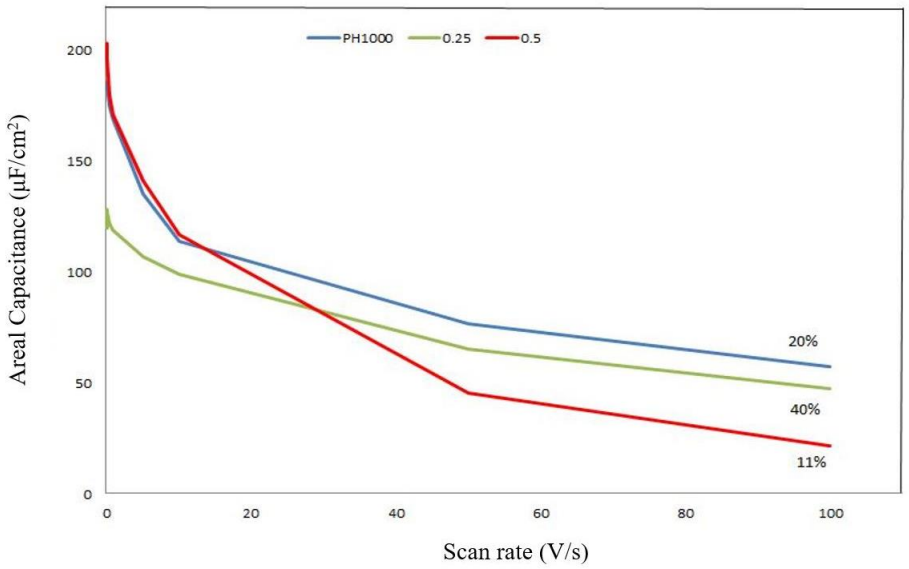

Fig.4-5, Areal capacitance vs scan rate and capacitance retention for devices 1-1(blue), 1-3 (green), and 1-4(red)

In most electrical double-layer capacitors, the carbon is generally pre-treated to remove the surface functional groups and moisture for capacitance and cycling improvement[54]. It has also been show that presence of oxygenated groups contributes to instability of the capacitor resulting in deterioration of capacitance and series of increase in resistance[15]. Taking all these into account and the fact that any pre-treatment on the porous carbon was performed, the reduction in the capacitance could be related to this matter. Also, the dispersion process of the porous carbon might not have been very successful. In the following images (Figs. 4-6 to 4-9), the atomic force microscopy (AFM) and scanning electron microscopy (SEM) characterization for device 1-4 (which had the highest amount of porous carbon) are illustrated.

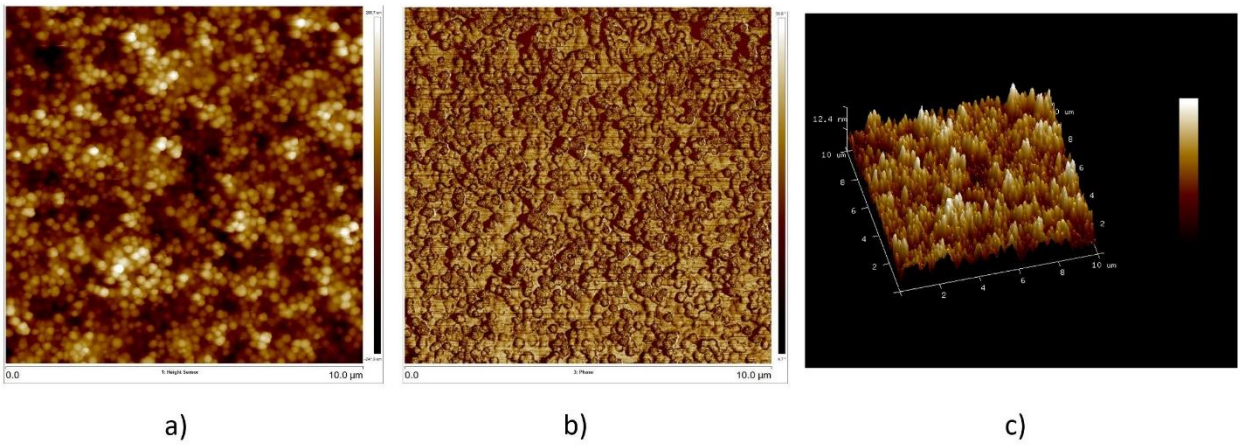

Fig.4-6, AFM characterization demonstrating a) topography b) phase and c) 3D image of hybrid ink of 50 -50 percent porous carbon and PH1000 deposited on SiO_2 substrate by spin coating.

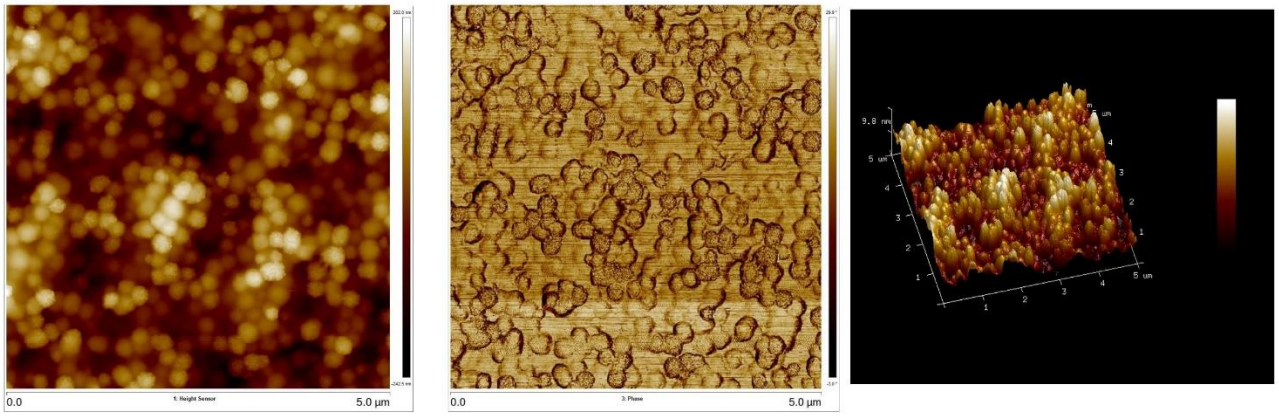

Fig.4-7, AFM characterization demonstrating 5 µm^2 area a) topography b) phase and c) 3D image of hybrid ink of 50 -50 percent porous carbon and PH1000 deposited on SiO_2 substrate by spin coating.

The AFM images of the hybrid film shows some surface roughness. In the 10 µm^2 overview (Fig. 4-6), the surface is not very smooth and in spite of long hours of stirring and sonication, carbon particles are seen in a form of bundles rather than being well-scattered across the surface. Especially in the 3D version of the images, the not very well-dispersed particles with heights up to 12 nm above the surface can be seen. In Fig.4-7 a smaller section (5µm^2), with an uneven surface is depicted.

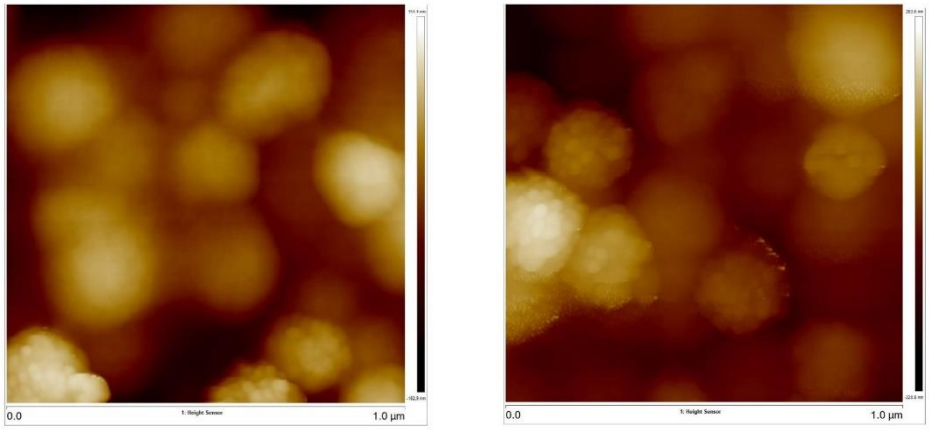

Fig.4-8, AFM characterization from hybrid ink of 50 -50 percent porous carbon and PH1000 deposited on SiO_2 substrate by spin coating.

When zoomed in to 1µm^2, the porous structure of the particles become visible (Fig.4-8) but to have a better view of the structure we examined the same sample with scanning electron microscopy.

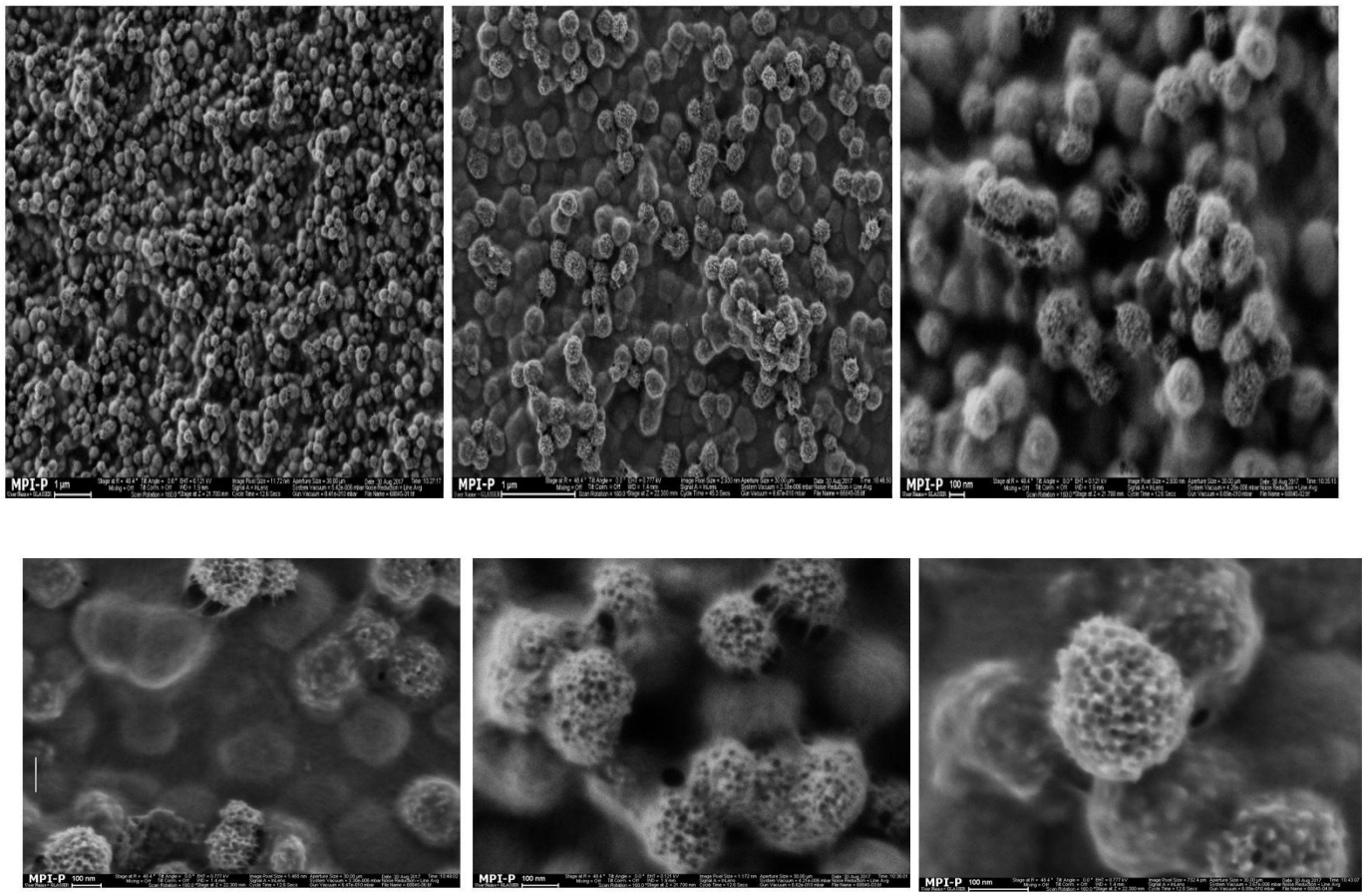

Fig.4-9, Scanning electron microscopy images with secondary electrons (SE) from PH1000 deposited on SiO_2 substrate by spin coating in different magnetizations.

To examine the morphology of the fabricated hybrid ink, scanning electron microscopy was conducted on the sample made from 50% porous carbon and 50% PH1000 on a SiO_2 substrate (Fig.4-9). The porous structure of the carbon particles are visible in the SEM images. However, most of these particles are agglomerated and not dispersed very well which is not beneficial for electron conduction. Also, being present in the form of agglomeration, it does not assist in increasing the accessible surface area which was the first point of introducing a porous structure to the polymer.

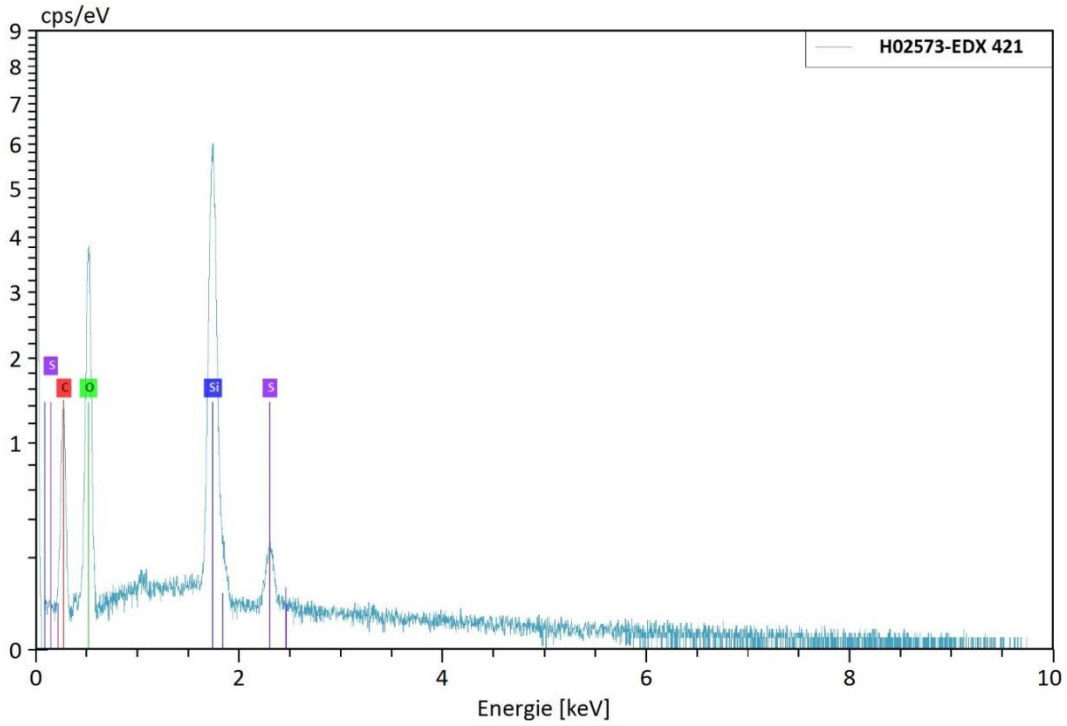

Fig.4-10, EDX characterization from PH1000 deposited on SiO_2 substrate by spin coating in different magnetizations.

Using the back-scattered electrons in SEM, EDX characterization gives us some information about the elements which are present in our sample (Fig. 4-10). Here, the firs visible peak is referred to sulfur which can be found in PH1000 structure (Fig. 4-11). Having SiO_2 substrate, the silicon peak is justified. Carbon and oxygen are both present in the PH1000 and the porous structure. Based on these results, we could not conclude any inconsistency with what was expected. There are no impurities or additional material that could be detected by EDX.

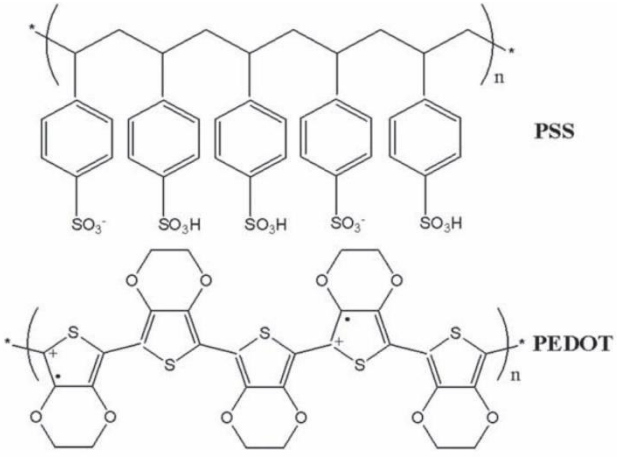

Fig.4-11, PH1000 structure

To make sure about the structure of the porous carbon, in the last step we used x-ray diffraction.

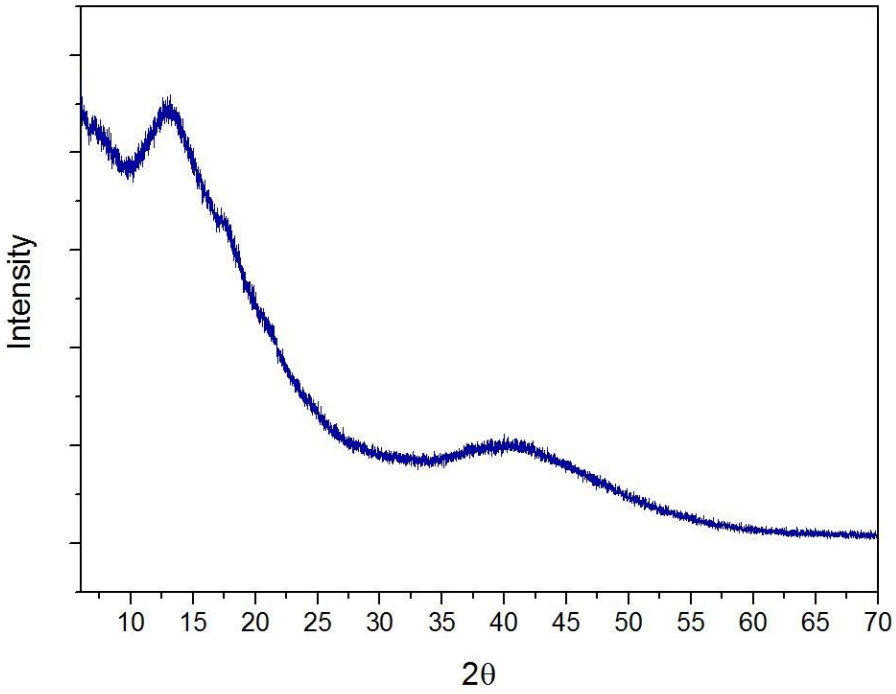

Fig.4-12, XRD pattern of porous carbon powder

Based on the X-ray pattern in Fig.4-12, the carbon powder has an amorphous behavior which explains the reason for lower conductivity and as a result lower capacitance than the polymer alone.

4. 2 Electrochemically Exfoliated Graphene/ RuO_2

In the second part of the project, MSCs were fabricated based on EG and RuO_2 trying to take advantage of both electrical double-layer and pseudo capacitance ability in both these materials.

Firstly a hybrid ink formed of the same amount of RuO_2 and EG was made and then making different concentrations in DMF of this ink (Table 2-2). The CV results from different concentrations (2,4 and 6 ml) are shown in the following Tables 4-6 to 4-12.

Table 4-6 CV results from pure sample 2-0

Scan Rate	Integral	Device Area(cm^2)	C_{area} ($\mu F/cm^2$)	Thickness (nm)	Volume (cm^3)	C_{volume} F/cm^3
0.01	5.19E-07	0.5	104	163	8.15E-06	6.36
0.05	2.49E-06	0.5	99.4	163	8.15E-06	6.1
0.1	4.79E-06	0.5	95.8	163	8.15E-06	5.87
0.5	2.17E-05	0.5	87	163	8.15E-06	5.33
1	4.13E-05	0.5	82.6	163	8.15E-06	5.06
5	1.72E-04	0.5	68.8	163	8.15E-06	4.21
10	2.96E-04	0.5	59.1	163	8.15E-06	3.62
50	9.58E-04	0.5	38.3	163	8.15E-06	2.35
100	1.61E-03	0.5	32.2	163	8.15E-06	1.97
200	0.00298	0.5	29.8	163	8.15E-06	1.82
1000	0.00806	0.5	16.1	163	8.15E-06	0.98

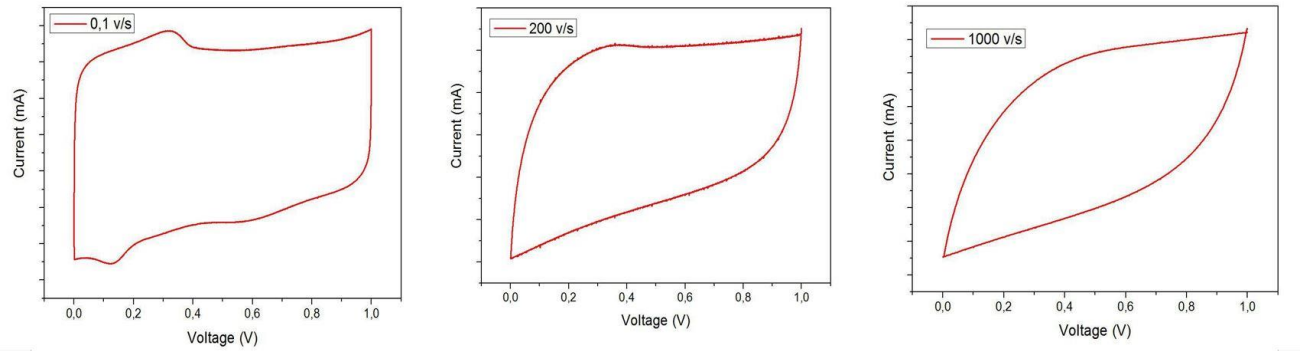

Fig.4-13, CV curves of sample 2-0 in 0.1, 200 and 1000 V/s scan rates

The CV curves for the pure sample 2-0 (Fig.4-13) are not rectangular and the areal capacitance decreases very rapidly by increasing the voltage rate in a way that at 1000 V/s the areal capacitance is only 16 μFcm^{-2} and volumetric capacitance is almost 1 Fcm^{-3}.

In the next steps RuO_2 was used to enhance the capacitance relying on the reversible redox reactions (pseudo-capacitive behavior) that can happen on the surface of this material [17] leading to

a better charge storage than that of carbon materials. According to the equation below, RuO_2 can change oxidation states between 2 to 5.

$$RuO_x(OH)_y + \delta H^+ + \delta e^- \Leftrightarrow RuO_{x-\delta}(OH)_{y+\delta}$$

Firstly, the same amount from the metal oxide and EG was used and the RuO_2 powder with EG was dispersed in DMF. By preparing multiple devices with different concentration of the same ink, each CV device performance was measured.

Table 4-7, CV results from sample 2-1

Scan Rate	Integral	Device Area(cm^2)	C_{area} ($\mu F/cm^2$)	Thickness (nm)	Volume (cm^3)	C_{volume} F/cm^3
0.01	9.03E-07	0.5	180.5693	170	0.0000085	10.62
0.05	5.02E-06	0.5	200.7026	170	0.0000085	11.80
0.1	9.71E-06	0.5	194.1237	170	0.0000085	11.41
0.5	4.76E-05	0.5	190.5278	170	0.0000085	11.20
1	9.11E-05	0.5	182.1839	170	0.0000085	10.71
5	3.86E-04	0.5	154.4186	170	0.0000085	9.08
10	6.72E-04	0.5	134.3523	170	0.0000085	7.90
50	0.002128	0.5	85.11114	170	0.0000085	5.006
100	0.003447	0.5	68.94116	170	0.0000085	4.05
200	0.005451	0.5	54.50857	170	0.0000085	3.206
1000	0.010887	0.5	21.77323	170	0.0000085	1.28

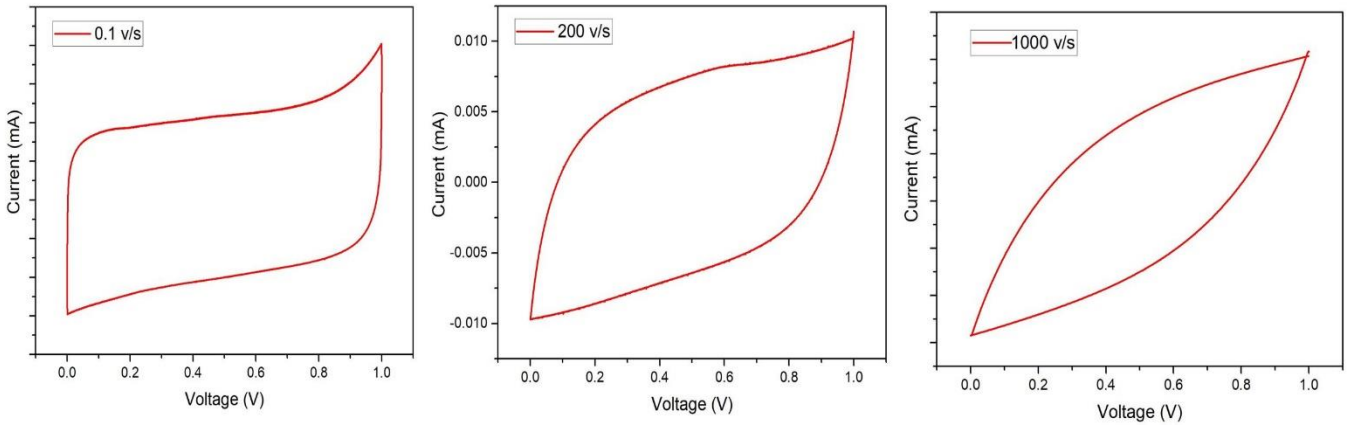

Fig.4-14, CV curves of sample 2-1 in 0.1, 200 and 1000 V/s scan rates

The most obvious difference between sample 2-0 and 2-1 is the shape of the CV curve with a very well-shaped hysteresis. The highest areal capacitance is 200 μFcm^{-2} at $50mVs^{-1}$ but still at ultrahigh voltage rate, the capacitance is very low compared to the methane reduced graphene oxide

based MSC previously reported[55]. With increasing concentration, capacitance also increases and so does the thickness which results in lower volumetric capacitance.

Table 4-8, CV results from sample 2-2

Scan Rate	Integral	Device Area(cm^2)	C_{area} ($\mu F/cm^2$)	Thickness (nm)	Volume (cm^3)	C_{volume} F/cm^3
0.01	1.12E-06	0.5	224	290	0.0000145	7.72
0.1	1.18E-05	0.5	236	290	0.0000145	8.13
0.5	5.71E-05	0.5	228.4	290	0.0000145	7.87
1	1.09E-04	0.5	218	290	0.0000145	7.51
5	4.67E-04	0.5	186.8	290	0.0000145	6.44
10	8.17E-04	0.5	163.4325	290	0.0000145	5.63
50	0.002658	0.5	106.3372	290	0.0000145	3.66
200	0.007244	0.5	72.43576	290	0.0000145	2.49
1000	0.013178	0.5	26.3558	290	0.0000145	0.90

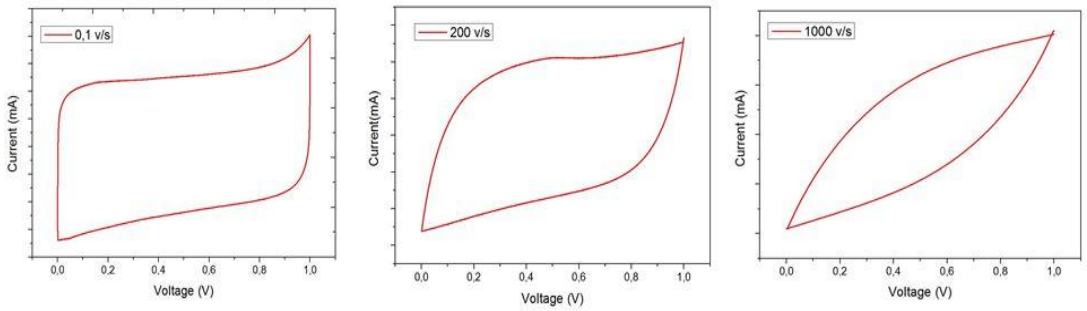

Fig.4-15, CV curves of sample 2-2 in 0.1, 200 and 1000 V/s scan rates

The highest concentration (sample 2-3) performs exceptionally better than the two last ones because of the lower thickness and also it can be related to the higher amount of EG. The CV curve still kept its almost rectangular shape indicative of electrical double layer while the deviation from the rectangular shape is indicative of pseudocapacitance.

Table 4-9, CV results from sample 2-3

Scan Rate	Integral	Device Area(cm^2)	C_{area} ($\mu F/cm^2$)	Thickness (nm)	Volume (cm^3)	C_{volume} F/cm^3
0.01	4.81E-06	0.5	961.1511	188	0.0000094	51.12
0.05	2.34E-05	0.5	937.738	188	0.0000094	49.87
0.1	4.30E-05	0.5	859.5072	188	0.0000094	45.71
0.5	2.00E-04	0.5	798.5597	188	0.0000094	42.47
1	3.60E-04	0.5	720.7455	188	0.0000094	38.33
5	0.001248	0.5	499.3662	188	0.0000094	26.56
10	0.002144	0.5	428.8886	188	0.0000094	22.81
50	0.007159	0.5	286.3715	188	0.0000094	15.23
100	0.010165	0.5	203.3016	188	0.0000094	10.81
200	0.013441	0.5	134.4055	188	0.0000094	7.149

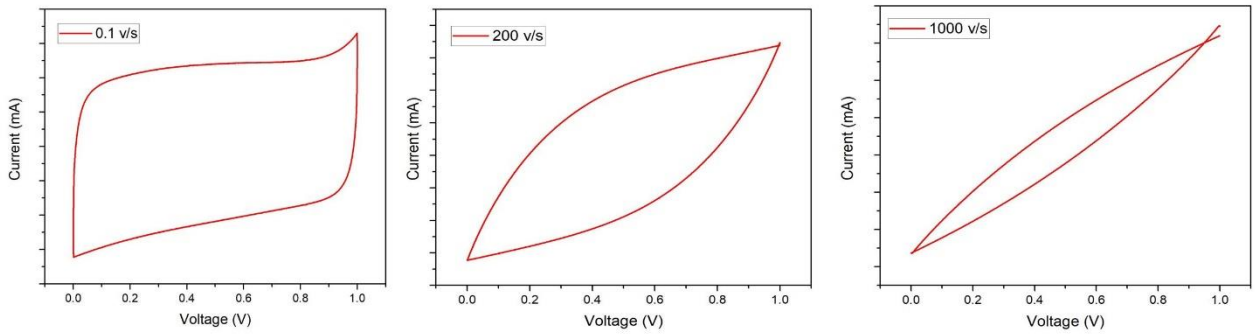

Fig.4-16, CV curves of sample 2-3 in 0.1, 200 and 1000 V/s scan rates

As depicted in Table 2-2, in samples 2-4 to 2-6 we decided to increase the amount of EG to 3 times more than RuO_2. Comparing the results with the same concentration and less amount of EG, the capacitance has increased from 180 μFcm^{-2} to 228 μFcm^{-2} at 10mVs^{-1} and it continues to be better by the same amount which proves that increasing EG improves the capacitance.

Table 4-10, CV results from sample 2-4

Scan Rate	Integral	Device Area(cm^2)	C_{area} ($\mu F/cm^2$)	Thickness (nm)	Volume (cm^3)	C_{volume} F/cm^3
0.01	1.14E-06	0.5	228	170	0.000085	1.34
0.05	8.14E-06	0.5	326	170	0.000085	1.91
0.1	1.54E-05	0.5	307	170	0.000085	1.80
0.5	7.69E-05	0.5	308	170	0.000085	1.80
1	1.39E-04	0.5	279	170	0.000085	1.63
5	4.89E-04	0.5	196	170	0.000085	1.15
10	8.37E-04	0.5	167	170	0.000085	0.98
50	0.002955	0.5	118	170	0.000085	0.69
100	0.002909	0.5	58.2	170	0.000085	0.34
200	0.006285	0.5	62.9	170	0.000085	0.36

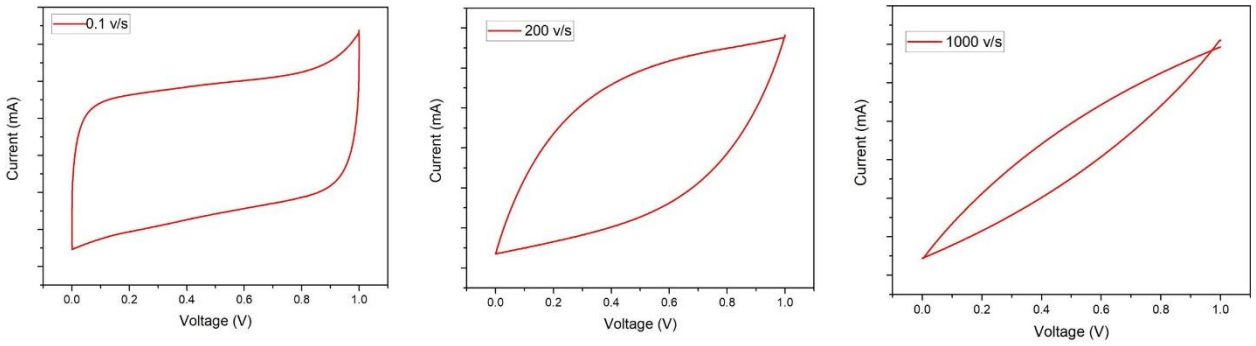

Fig.4-17, CV curves of sample 2-4 in 0.1, 200 and 1000 V/s scan rates

Increasing the concentration (sample 2-5), the areal and volumetric capacitance both increased compared to the same concentration with less amount of RuO_2. Compared to 2-1 sample, the areal capacitance has increased but volumetric capacitance is about the same amount which is related to the fact that the thickness has also increased more than 100 nm.

Table 4-11, CV results from sample 2-5

Scan Rate	Integral	Device Area(cm^2)	C_{area} ($\mu F/cm^2$)	Thickness (nm)	Volume (cm^3)	C_{volume} F/cm^3
0.01	3.81E-06	0.5	761	290	0.000145	2.62
0.05	2.06E-05	0.5	823	290	0.000145	2.83
0.1	4.05E-05	0.5	810	290	0.000145	2.79
0.5	1.87E-04	0.5	748	290	0.000145	2.57
1	3.52E-04	0.5	703	290	0.000145	2.42
5	0.001348	0.5	539	290	0.000145	1.85
10	0.002268	0.5	454	290	0.000145	1.56
50	0.007131	0.5	285	290	0.000145	0.98
100	0.010747	0.5	215	290	0.000145	0.74
200	0.013873	0.5	139	290	0.000145	0.47

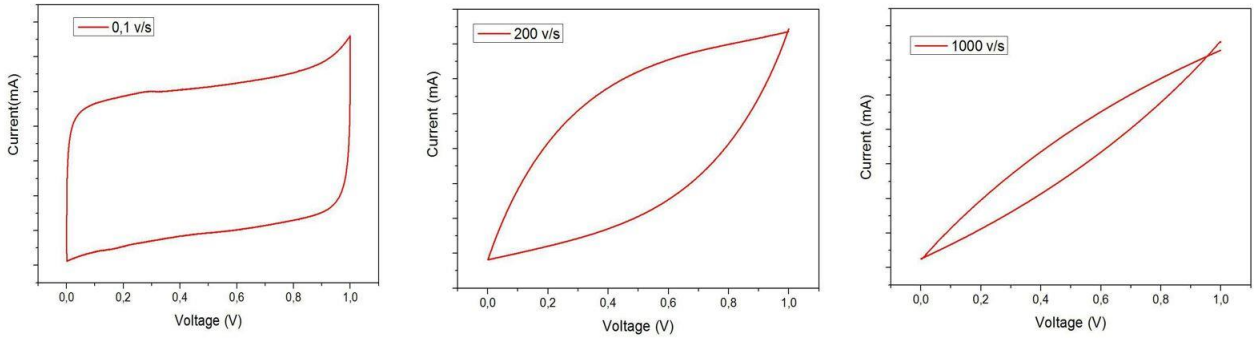

Fig.4-18, CV curves of sample 2-5 in 0.1, 200 and 1000 V/s scan rates

In the last step of concentration increase (sample 2-6), similar to sample 2-3, it is observed the best areal capacitance especially in lower scan rates which goes up to 1.05 $mFcm^{-2}$ which is comparable to MSCs based on mesoporous polyaniline patterned graphene [56], however the volumetric capacitance is not as high.

Table 4-12, CV results from sample 2-6

Scan Rate	Integral	Device Area(cm^2)	C_{area} ($\mu F/cm^2$)	Thickness (nm)	Volume (cm^3)	C_{volume} F/cm^3
0.01	5.06E-06	0.5	1010	354	0.000177	2.85
0.05	2.62E-05	0.5	1050	354	0.000177	2.963
0.1	5.38E-05	0.5	1080	354	0.000177	3.037
0.5	2.45E-04	0.5	980	354	0.000177	2.76
1	4.70E-04	0.5	939	354	0.000177	2.65
5	0.001921	0.5	768	354	0.000177	2.17
10	0.003242	0.5	648	354	0.000177	1.83
50	0.00843	0.5	337	354	0.000177	0.95
100	0.011004	0.5	220	354	0.000177	0.62
200	0.012021	0.5	120	354	0.000177	0.33

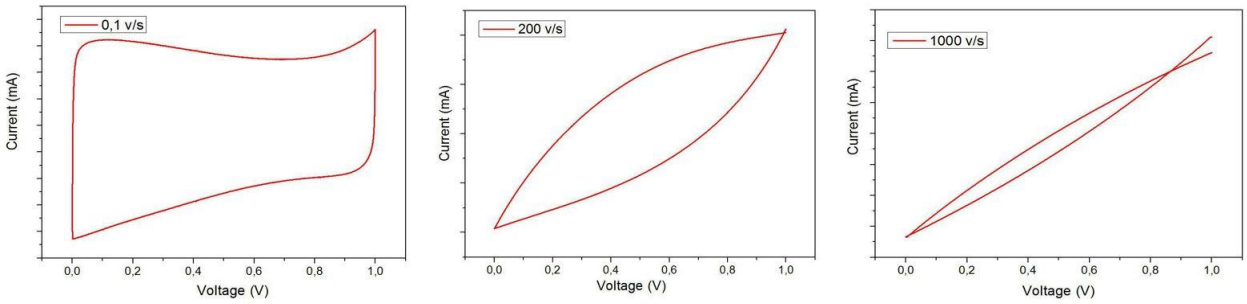

Fig.4-19, CV curves of sample 2-6 in 0.1, 200 and 1000 V/s scan rates

In this sample which had the best results compared to the rest, AFM analysis was performed. Images from 5 μm^2 (Fig. 4-20) and 1μm^2 (Fig. 4-21) cross-section of the sample were taken to examine the surface structure.

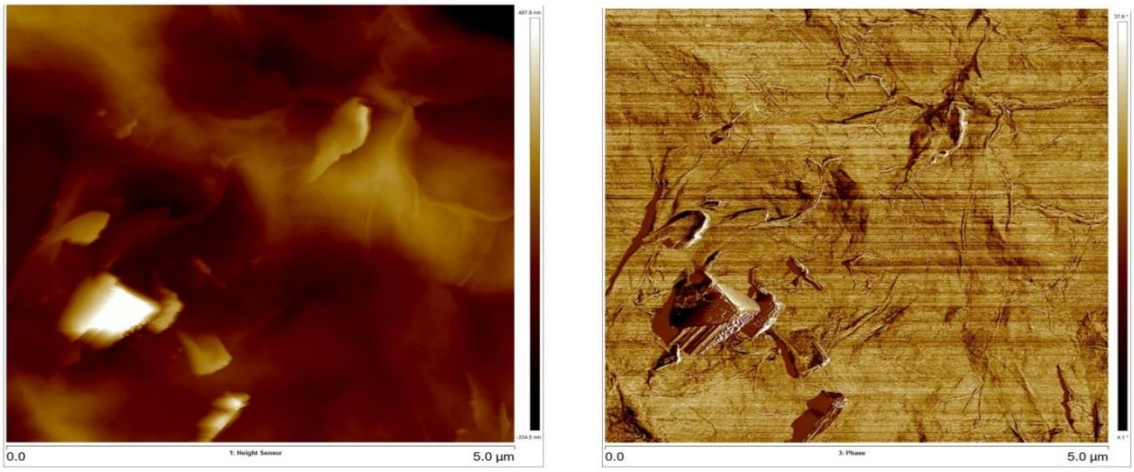

Fig.4-20, AFM characterization from sample 2-6 in a) topography and b) phase mode

In the overview from 5µm^2 cross-section, we can see the graphene layers as well as piece of RuO_2 which is present in a form of a comparably big agglomerated piece.

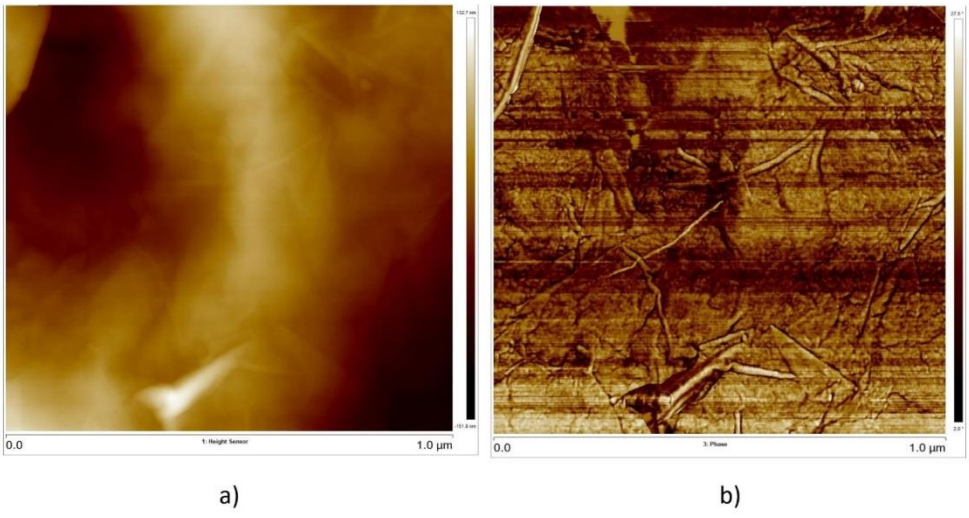

Fig.4-21, AFM characterization from sample 2-6 in a) topography and b) phase mode

In the smaller cross-section, the graphene layer can be seen with a rather smooth surface which does not have many wrinkles which is beneficial for electron conduction. Still, RuO_2 is only

visible in a form of an agglomeration. Since the original RuO_2 nanosheets were mostly stuck together and it could be concluded that a proper dispersion of the RuO_2 nanosheets did not happen.

The sample was also characterized by SEM and the images with different magnifications are illustrated in the following Figs. 4-22 to 4-25.

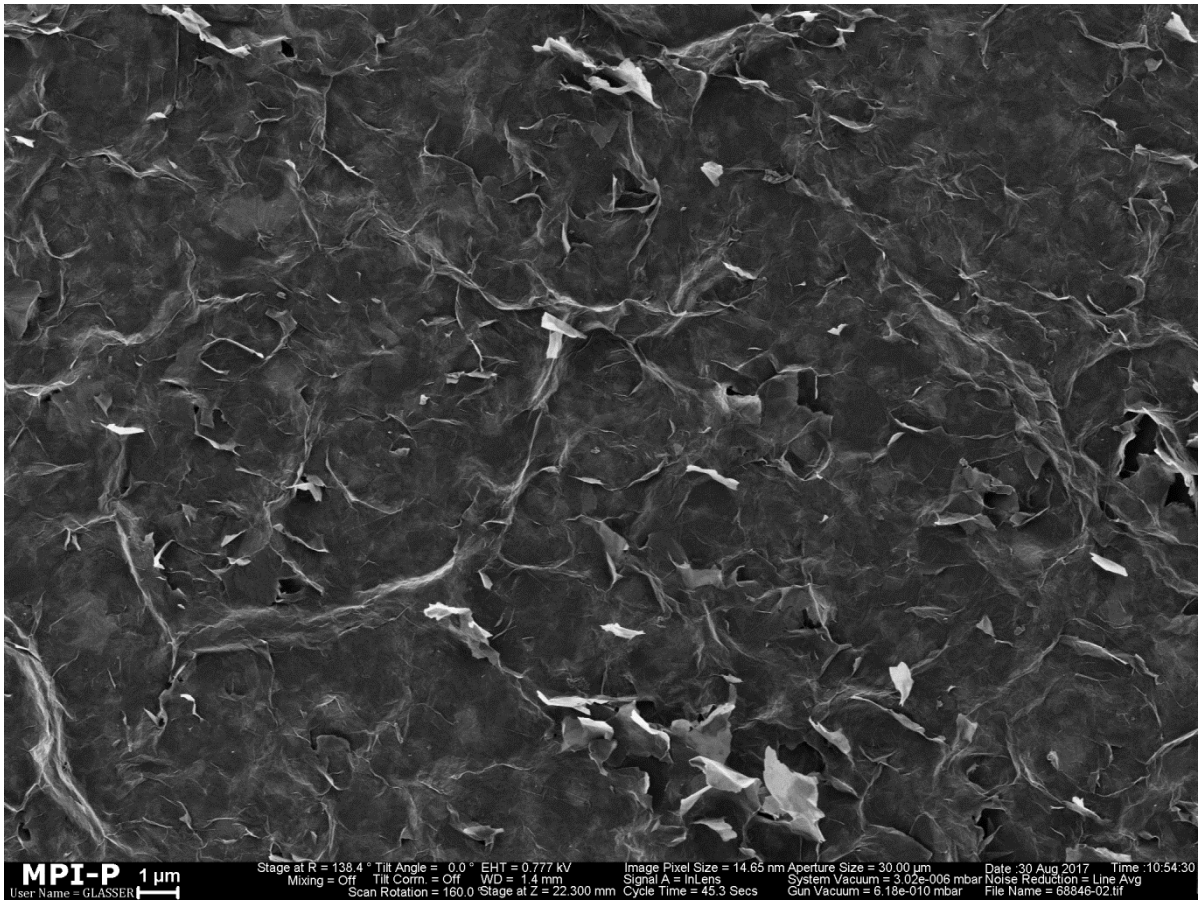

Fig.4-22, SEM image from sample 2-6

RuO_2 particles (white contrast) as big as 1µm can be seen in the images, namely by zooming into the small particles, the size can be estimated to about 200 nm. These particles are not evenly dispersed across the surface and the surface is not very smooth. Roughness of the surface as well as the presence of the big particles hinder the electron conductivity the later also means that the contact surface area between EG and RuO_2 is not efficient.

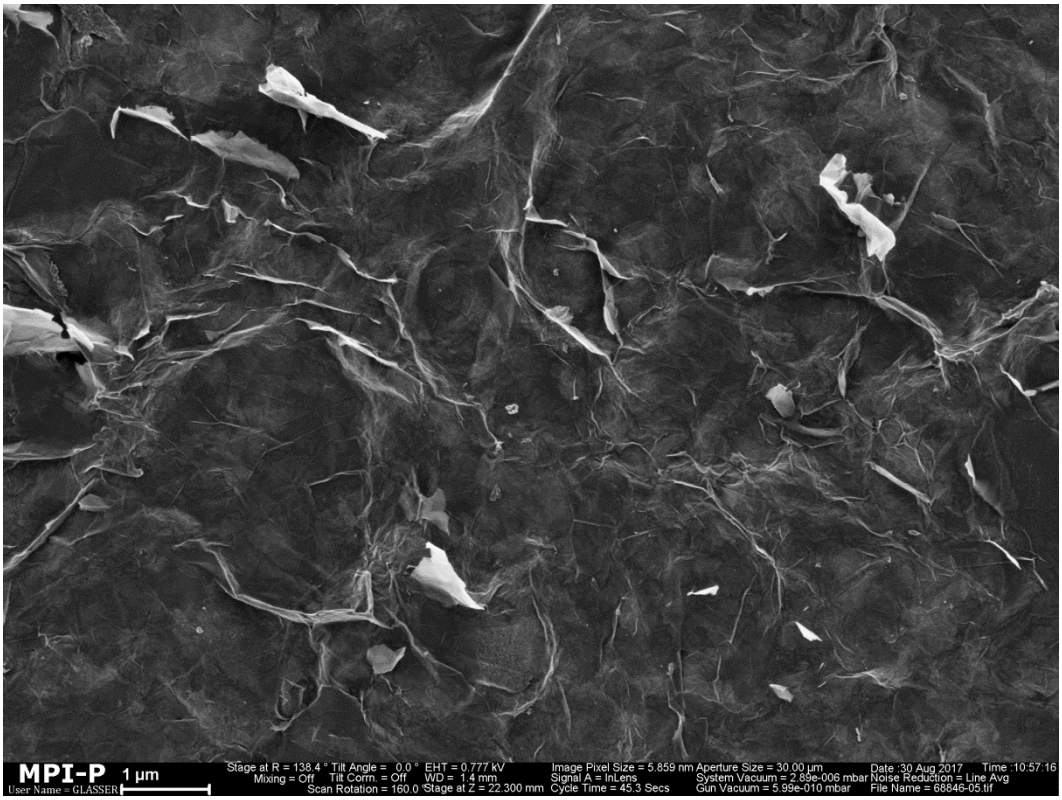

Fig.4-23, SEM image from sample 2-6

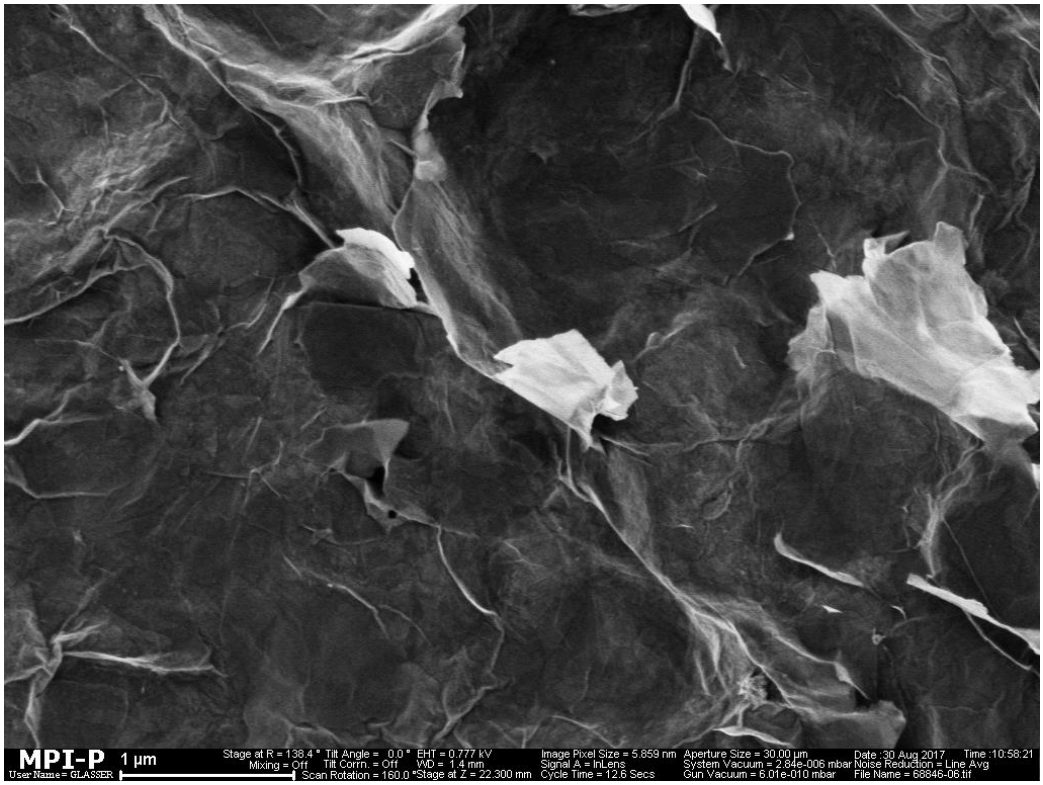

Fig.4-24, SEM image from sample 2-6

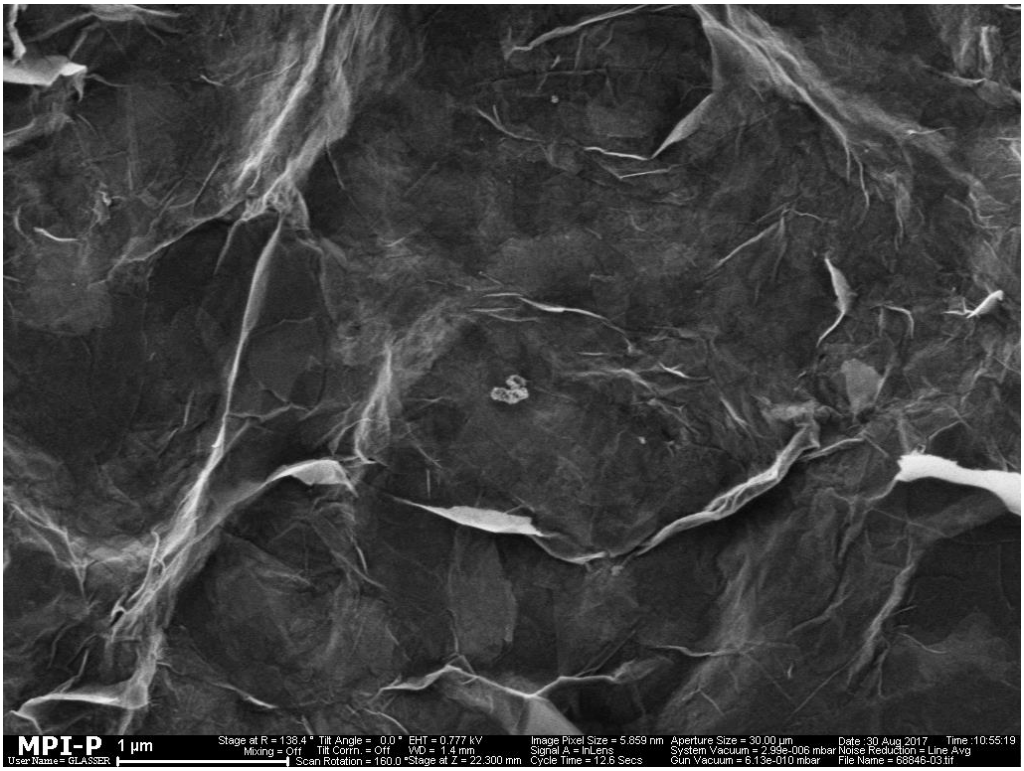

Fig.4-25, SEM image from sample 2-6

Based on EDX characterization (Fig.4-26), the peaks are related to Ruthenium, Oxygen and Carbon. The presence of a weak sodium peak can be related to the fact that RuO_2 nanosheets are made from exfoliation of $Na_{0.2}RuO_2$.

In the last step, the XRD pattern from the RuO_2 nanosheets was examined and, surprisingly, it looked different from what was reported before [46] and it showed a complete amorphous behavior.

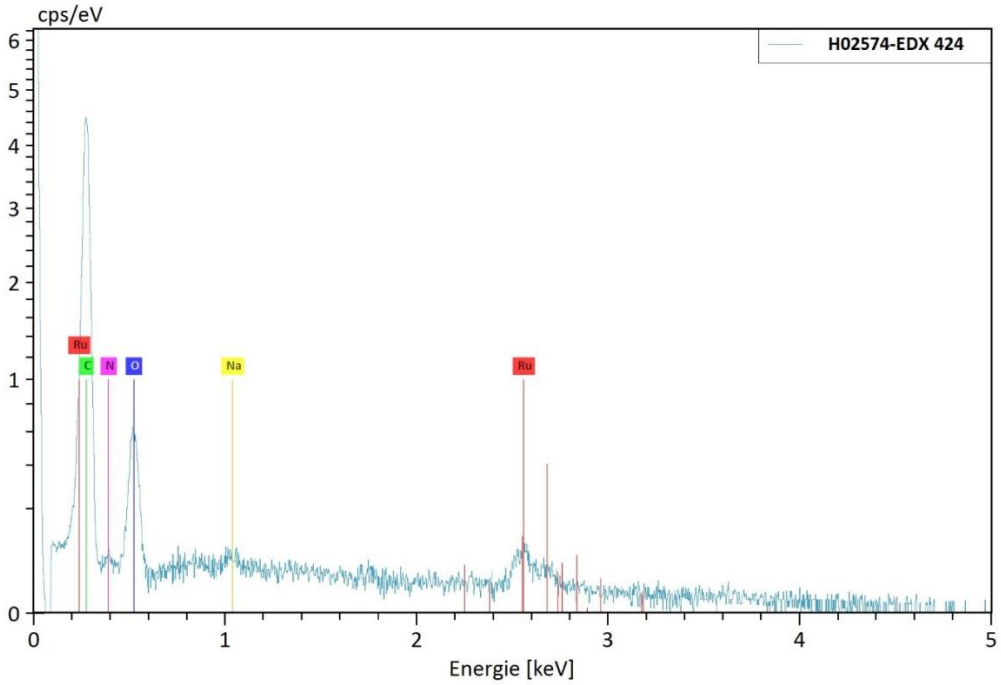

Fig.4-26, EDX characterization of sample 2-6

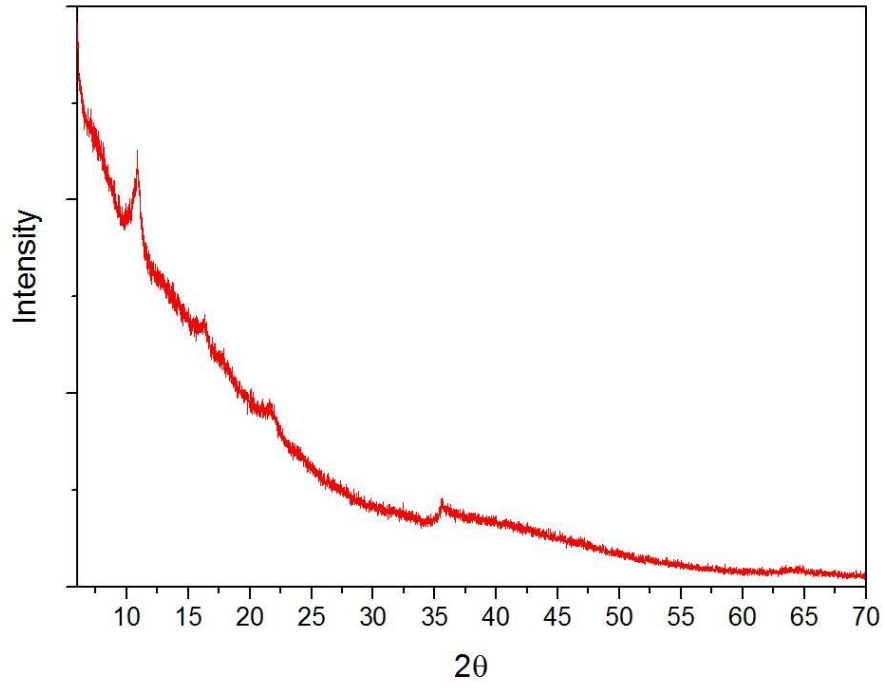

Fig.4-27, XRD pattern from RuO_2 nanosheets

Chapter 5

Conclusion and Future Prospect

In this work, micro-supercapacitors based on hybrid inks combining both electrical double-layer and pseudocapacitance were prepared. Dividing the project in two parts, in the first part a hybrid ink was prepared using a conductive polymer (PH1000) and mesoporous carbon spheres with high specific surface area. In the second part, the hybrid ink was based on electrochemically exfoliated graphene and RuO_2 nanosheets.

In each part MSC devices were successfully prepared using suited method for deposition of the electrode layer and Au collectors were deposited in both cases. PVA/H_2SO_4 gel was used as the electrolyte because of its ability to solidify fast and as a result avoiding the usage of liquid electrolytes and their harmful leakages.

Based on the results from x-ray diffraction, both mesoporous carbon and RuO_2 powder had amorphous behavior which is the main reason that the results from areal and volumetric capacitance were not as it was expected. This amorphous structure has a big influence on decreasing the electronic conductivity.

In the first part, areal capacitance up to 203 μFcm^{-2} and volumetric capacitance up to $12Fcm^{-3}$ at $10mVs^{-1}$ was achieved. Reducing the electrode thickness will result in higher amounts of volumetric capacitance and for this matter it is suggested to increase the spin-coating speed in order to achieve a thinner layer. The SEM and AFM results both showed a rough surface with mesoporous carbon particles mostly present in agglomerated condition, better dispersion of the powder will result in better conductivity and also smoother surface and less thickness.

In the second part the areal capacitance went up to 1 $mFcm^{-2}$ with volumetric capacitance of 51 Fcm^{-3} at $10mVs^{-1}$ which is comparable to the best graphene-based MSCs reported so far. Reducing the device thickness as well as better dispersion of the RuO_2 nanosheets will improve the performance significantly.

Bibliography:

1. Miller, J.R. and P. Simon, *Electrochemical capacitors for energy management.* Science Magazine, 2008. **321**(5889): p. 651-652.
2. Stoller, M.D., S. Park, Y. Zhu, J. An, and R.S. Ruoff, *Graphene-based ultracapacitors.* Nano letters, 2008. **8**(10): p. 3498-3502.
3. Hashmi, S., *Supercapacitor: an emerging power source.* National Academy Science Letters, 2004. **27**(1-2): p. 27-46.
4. Kötz, R. and M. Carlen, *Principles and applications of electrochemical capacitors.* Electrochimica acta, 2000. **45**(15): p. 2483-2498.
5. Chmiola, J., G. Yushin, Y. Gogotsi, C. Portet, P. Simon, and P.-L. Taberna, *Anomalous increase in carbon capacitance at pore sizes less than 1 nanometer.* Science, 2006. **313**(5794): p. 1760-1763.
6. Conway, B.E., *Transition from "supercapacitor" to "battery" behavior in electrochemical energy storage.* Journal of the Electrochemical Society, 1991. **138**(6): p. 1539-1548.
7. Rolison, D.R., J.W. Long, J.C. Lytle, A.E. Fischer, C.P. Rhodes, T.M. McEvoy, M.E. Bourg, and A.M. Lubers, *Multifunctional 3D nanoarchitectures for energy storage and conversion.* Chemical Society Reviews, 2009. **38**(1): p. 226-252.
8. Arthur, T.S., D.J. Bates, N. Cirigliano, D.C. Johnson, P. Malati, J.M. Mosby, E. Perre, M.T. Rawls, A.L. Prieto, and B. Dunn, *Three-dimensional electrodes and battery architectures.* Mrs Bulletin, 2011. **36**(7): p. 523-531.
9. Chmiola, J., C. Largeot, P.-L. Taberna, P. Simon, and Y. Gogotsi, *Monolithic carbide-derived carbon films for micro-supercapacitors.* Science, 2010. **328**(5977): p. 480-483.
10. Zhai, Y., Y. Dou, D. Zhao, P.F. Fulvio, R.T. Mayes, and S. Dai, *Carbon materials for chemical capacitive energy storage.* Advanced materials, 2011. **23**(42): p. 4828-4850.
11. Wu, Z.-S., G. Zhou, L.-C. Yin, W. Ren, F. Li, and H.-M. Cheng, *Graphene/metal oxide composite electrode materials for energy storage.* Nano Energy, 2012. **1**(1): p. 107-131.
12. Wu, Z.-S., Y. Sun, Y.-Z. Tan, S. Yang, X. Feng, and K. Müllen, *Three-dimensional graphene-based macro-and mesoporous frameworks for high-performance electrochemical capacitive energy storage.* Journal of the American Chemical Society, 2012. **134**(48): p. 19532-19535.
13. Bonaccorso, F., L. Colombo, G. Yu, M. Stoller, V. Tozzini, A.C. Ferrari, R.S. Ruoff, and V. Pellegrini, *Graphene, related two-dimensional crystals, and hybrid systems for energy conversion and storage.* Science, 2015. **347**(6217): p. 1246501.
14. Zhang, S. and N. Pan, *Supercapacitors performance evaluation.* Advanced Energy Materials, 2015. **5**(6).
15. Pandolfo, A. and A. Hollenkamp, *Carbon properties and their role in supercapacitors.* Journal of power sources, 2006. **157**(1): p. 11-27.
16. Simon, P. and Y. Gogotsi, *Materials for electrochemical capacitors.* Nature materials, 2008. **7**(11): p. 845-854.
17. Wu, N.-L., *Nanocrystalline oxide supercapacitors.* Materials Chemistry and Physics, 2002. **75**(1): p. 6-11.
18. Brousse, T., M. Toupin, R. Dugas, L. Athouël, O. Crosnier, and D. Bélanger, *Crystalline MnO2 as possible alternatives to amorphous compounds in electrochemical supercapacitors.* Journal of The Electrochemical Society, 2006. **153**(12): p. A2171-A2180.
19. Liu, T., L. Finn, M. Yu, H. Wang, T. Zhai, X. Lu, Y. Tong, and Y. Li, *Polyaniline and polypyrrole pseudocapacitor electrodes with excellent cycling stability.* Nano letters, 2014. **14**(5): p. 2522-2527.
20. Gao, W., N. Singh, L. Song, Z. Liu, A.L.M. Reddy, L. Ci, R. Vajtai, Q. Zhang, B. Wei, and P.M. Ajayan, *Direct laser writing of micro-supercapacitors on hydrated graphite oxide films.* Nature nanotechnology, 2011. **6**(8): p. 496-500.
21. Pech, D., M. Brunet, H. Durou, P. Huang, V. Mochalin, Y. Gogotsi, P.-L. Taberna, and P. Simon, *Ultrahigh-power micrometre-sized supercapacitors based on onion-like carbon.* Nature nanotechnology, 2010. **5**(9): p. 651-654.

22. El-Kady, M.F. and R.B. Kaner, *Scalable fabrication of high-power graphene micro-supercapacitors for flexible and on-chip energy storage.* Nature communications, 2013. **4**: p. 1475.
23. Wu, Z.S., K. Parvez, X. Feng, and K. Müllen, *Graphene-based in-plane micro-supercapacitors with high power and energy densities.* Nature communications, 2013. **4**.
24. Pech, D., M. Brunet, T.M. Dinh, K. Armstrong, J. Gaudet, and D. Guay, *Influence of the configuration in planar interdigitated electrochemical micro-capacitors.* Journal of Power Sources, 2013. **230**: p. 230-235.
25. Qi, D., Y. Liu, Z. Liu, L. Zhang, and X. Chen, *Design of Architectures and Materials in In-Plane Micro-supercapacitors: Current Status and Future Challenges.* Advanced Materials, 2016.
26. Meng, F. and Y. Ding, *Sub-Micrometer-Thick All-Solid-State Supercapacitors with High Power and Energy Densities.* Advanced Materials, 2011. **23**(35): p. 4098-4102.
27. Beidaghi, M. and C. Wang, *Micro-supercapacitors based on interdigital electrodes of reduced graphene oxide and carbon nanotube composites with ultrahigh power handling performance.* Advanced Functional Materials, 2012. **22**(21): p. 4501-4510.
28. Li, Z., G. Ma, R. Ge, F. Qin, X. Dong, W. Meng, T. Liu, J. Tong, F. Jiang, and Y. Zhou, *Free-Standing Conducting Polymer Films for High-Performance Energy Devices.* Angewandte Chemie, 2016. **128**(3): p. 991-994.
29. Liu, C.-C., D.-S. Tsai, D. Susanti, W.-C. Yeh, Y.-S. Huang, and F.-J. Liu, *Planar ultracapacitors of miniature interdigital electrode loaded with hydrous RuO 2 and RuO 2 nanorods.* Electrochimica Acta, 2010. **55**(20): p. 5768-5774.
30. Xue, M., Z. Xie, L. Zhang, X. Ma, X. Wu, Y. Guo, W. Song, Z. Li, and T. Cao, *Microfluidic etching for fabrication of flexible and all-solid-state micro supercapacitor based on MnO 2 nanoparticles.* Nanoscale, 2011. **3**(7): p. 2703-2708.
31. Hughes, M., M.S. Shaffer, A.C. Renouf, C. Singh, G.Z. Chen, D.J. Fray, and A.H. Windle, *Electrochemical capacitance of nanocomposite films formed by coating aligned arrays of carbon nanotubes with polypyrrole.* Advanced Materials, 2002. **14**(5): p. 382-385.
32. Geim, A.K. and K.S. Novoselov, *The rise of graphene.* Nature materials, 2007. **6**(3): p. 183-191.
33. Yang, S., S. Brüller, Z.-S. Wu, Z. Liu, K. Parvez, R. Dong, F. Richard, P. Samorì, X. Feng, and K. Müllen, *Organic radical-assisted electrochemical exfoliation for the scalable production of high-quality graphene.* J. Am. Chem. Soc, 2015. **137**(43): p. 13927-13932.
34. Reina, A., X. Jia, J. Ho, D. Nezich, H. Son, V. Bulovic, M.S. Dresselhaus, and J. Kong, *Large area, few-layer graphene films on arbitrary substrates by chemical vapor deposition.* Nano letters, 2008. **9**(1): p. 30-35.
35. Novoselov, K.S., A.K. Geim, S.V. Morozov, D. Jiang, Y. Zhang, S.V. Dubonos, I.V. Grigorieva, and A.A. Firsov, *Electric field effect in atomically thin carbon films.* science, 2004. **306**(5696): p. 666-669.
36. Zhi, L. and K. Müllen, *A bottom-up approach from molecular nanographenes to unconventional carbon materials.* Journal of Materials Chemistry, 2008. **18**(13): p. 1472-1484.
37. Zhu, Y., S. Murali, W. Cai, X. Li, J.W. Suk, J.R. Potts, and R.S. Ruoff, *Graphene and graphene oxide: synthesis, properties, and applications.* Advanced materials, 2010. **22**(35): p. 3906-3924.
38. Yoo, J.J., K. Balakrishnan, J. Huang, V. Meunier, B.G. Sumpter, A. Srivastava, M. Conway, A.L. Mohana Reddy, J. Yu, and R. Vajtai, *Ultrathin planar graphene supercapacitors.* Nano letters, 2011. **11**(4): p. 1423-1427.
39. Xia, Y., K. Sun, and J. Ouyang, *Solution-processed metallic conducting polymer films as transparent electrode of optoelectronic devices.* Advanced Materials, 2012. **24**(18): p. 2436-2440.
40. Hu, C.-C., K.-H. Chang, M.-C. Lin, and Y.-T. Wu, *Design and tailoring of the nanotubular arrayed architecture of hydrous RuO2 for next generation supercapacitors.* Nano letters, 2006. **6**(12): p. 2690-2695.
41. Conway, B., V. Birss, and J. Wojtowicz, *The role and utilization of pseudocapacitance for energy storage by supercapacitors.* Journal of Power Sources, 1997. **66**(1-2): p. 1-14.
42. Wang, G., Y. Sun, D. Li, W. Wei, X. Feng, and K. Müllen, *Constructing Hierarchically Hollow Core–Shell MnO2/C Hybrid Spheres for High-Performance Lithium Storage.* Small, 2016. **12**(29): p. 3914-3919.

43. Parvez, K., Z.-S. Wu, R. Li, X. Liu, R. Graf, X. Feng, and K. Müllen, *Exfoliation of graphite into graphene in aqueous solutions of inorganic salts.* J. Am. Chem. Soc, 2014. **136**(16): p. 6083-6091.
44. Parvez, K., R. Li, S.R. Puniredd, Y. Hernandez, F. Hinkel, S. Wang, X. Feng, and K. Müllen, *Electrochemically exfoliated graphene as solution-processable, highly conductive electrodes for organic electronics.* 2013.
45. Shim, J., J.M. Yun, T. Yun, P. Kim, K.E. Lee, W.J. Lee, R. Ryoo, D.J. Pine, G.-R. Yi, and S.O. Kim, *Two-minute assembly of pristine large-area graphene based films.* Nano letters, 2014. **14**(3): p. 1388-1393.
46. Lee, S., X. Jin, I.Y. Kim, T.-H. Gu, J.-W. Choi, S. Nahm, and S.-J. Hwang, *Superior Additive of Exfoliated RuO2 Nanosheet for Optimizing the Electrode Performance of Metal Oxide over Graphene.* The Journal of Physical Chemistry C, 2016. **120**(22): p. 11786-11796.
47. Klein, A., S. Tiefenbacher, V. Eyert, C. Pettenkofer, and W. Jaegermann, *Electronic band structure of single-crystal and single-layer WS 2: Influence of interlayer van der Waals interactions.* Physical Review B, 2001. **64**(20): p. 205416.
48. D'Antò, V., R. Rongo, G. Ametrano, G. Spagnuolo, P. Manzo, R. Martina, S. Paduano, and R. Valletta, *Evaluation of surface roughness of orthodontic wires by means of atomic force microscopy.* The Angle Orthodontist, 2012. **82**(5): p. 922-928.
49. Werner, W.S., *Electron transport in solids for quantitative surface analysis.* Surface and Interface Analysis, 2001. **31**(3): p. 141-176.
50. Goodhew, P.J., J. Humphreys, and R. Beanland, *Electron microscopy and analysis*. 2000: CRC Press.
51. Hammond, C. and C. Hammond, *Basics of crystallography and diffraction*. Vol. 214. 2001: Oxford.
52. ChemViews, *100th Anniversary of the Discovery of X-ray Diffraction.* ChemistryViews, 2012.
53. Zhang, M., Q. Zhou, J. Chen, X. Yu, L. Huang, Y. Li, C. Li, and G. Shi, *An ultrahigh-rate electrochemical capacitor based on solution-processed highly conductive PEDOT: PSS films for AC line-filtering.* Energy & Environmental Science, 2016. **9**(6): p. 2005-2010.
54. Azaïs, P., L. Duclaux, P. Florian, D. Massiot, M.-A. Lillo-Rodenas, A. Linares-Solano, J.-P. Peres, C. Jehoulet, and F. Béguin, *Causes of supercapacitors ageing in organic electrolyte.* Journal of power sources, 2007. **171**(2): p. 1046-1053.
55. Wu, Z.S., K. Parvez, S. Li, S. Yang, Z. Liu, S. Liu, X. Feng, and K. Müllen, *Alternating Stacked Graphene-Conducting Polymer Compact Films with Ultrahigh Areal and Volumetric Capacitances for High-Energy Micro-Supercapacitors.* Advanced Materials, 2015. **27**(27): p. 4054-4061.
56. Liu, Z., S. Liu, R. Dong, S. Yang, H. Lu, A. Narita, X. Feng, and K. Müllen, *High Power In-Plane Micro-Supercapacitors Based on Mesoporous Polyaniline Patterned Graphene.* Small, 2017. **13**(14).